## Title

Klotho gene silencing promotes pathology in the mdx mouse model of Duchenne muscular dystrophy



## Journal

Human Molecular Genetics, 25(12)

## ISSN

0964-6906

## Authors

Wehling-Henricks, Michelle
Li, Zhenzhi
Lindsey, Catherine
et al.

## Publication Date

2016-06-15

## DOI

10.1093/hmg/ddw111

Peer reviewed

*Human Molecular Genetics*, 2016, Vol. 25, No. 12 2465–2482

**doi: 10.1093/hmg/ddw111**
Advance Access Publication Date: 6 May 2016
Original Article

ORIGINAL ARTICLE

# Klotho gene silencing promotes pathology in the *mdx* mouse model of Duchenne muscular dystrophy

Michelle Wehling-Henricks[1], Zhenzhi Li[1], Catherine Lindsey[1], Ying Wang[2], Steven S. Welc[1], Julian N. Ramos[1], Négar Khanlou[3], Makoto Kuro-o[4] and James G. Tidball[1,2,3,*]

[1]Department of Integrative Biology and Physiology, [2]Molecular, Cellular & Integrative Physiology Program, University of California, Los Angeles, CA 90095-1606, USA, [3]Department of Pathology and Laboratory Medicine, David Geffen School of Medicine at UCLA, University of California, Los Angeles, CA 90095-1732, USA and [4]Division of Anti-Aging Medicine, Center for Molecular Medicine, Jichi Medical University, 3311-1 Yakushiji, Shimotsuke, Tochigi 329-0498, Japan

*To whom correspondence should be addressed. Tel: +310 2063395; Fax: +310 8258489; Email: jtidball@physci.ucla.edu

## Abstract

Duchenne muscular dystrophy (DMD) is a lethal muscle disease involving progressive loss of muscle regenerative capacity and increased fibrosis. We tested whether epigenetic silencing of the *klotho* gene occurs in the *mdx* mouse model of DMD and whether *klotho* silencing is an important feature of the disease. Our findings show that *klotho* undergoes muscle-specific silencing at the acute onset of *mdx* pathology. *Klotho* experiences increased methylation of CpG sites in its promoter region, which is associated with gene silencing, and increases in a repressive histone mark, H3K9me2. Expression of a *klotho* transgene in *mdx* mice restored their longevity, reduced muscle wasting, improved function and greatly increased the pool of muscle-resident stem cells required for regeneration. Reductions of fibrosis in late, progressive stages of the *mdx* pathology achieved by transgene expression were paralleled by reduced expression of Wnt target genes (axin-2), transforming growth factor-beta (TGF-β1) and collagens types 1 and 3, indicating that Klotho inhibition of the profibrotic Wnt/TGFβ axis underlies its anti-fibrotic effect in aging, dystrophic muscle. Thus, epigenetic silencing of *klotho* during muscular dystrophy contributes substantially to lost regenerative capacity and increased fibrosis of dystrophic muscle during late progressive stages of the disease.

## Introduction

The discovery that Duchenne muscular dystrophy (DMD) is caused by mutation of the dystrophin gene that encodes a membrane associated structural protein (1) initially led to the expectation that the pathogenesis of DMD would be easily interpretable in the context of dystrophin-deficiency. However, the pathology of dystrophin-deficiency is intertwined with multiple secondary defects that play major roles in determining the magnitude and course of the disease. In part, the complexity of dystrophinopathies is attributable to the reduced stability and subsequent loss of a complex of dystrophin-associated proteins that serves structural, signaling and likely many unknown, regulatory functions in muscle (2). The complexity is also amplified by tremendous reductions in the expression of enzymes such as neuronal nitric oxide synthase [nNOS (3–5)] that play multiple and diverse regulatory roles in maintaining muscle homeostasis

**Received:** December 22, 2015. **Revised:** March 10, 2016. **Accepted:** April 8, 2016

and by the secondary involvement of other tissues, especially the immune system, that can play pivotal roles in determining the magnitude and course of the disease (6).

More recent discoveries have shown that perturbations in epigenetic regulation of gene expression also feature in the pathology of DMD and the *mdx* mouse model of DMD. For example, assays for global histone modifications in DMD and *mdx* muscles showed that histone H3 modifications including Lys 79 methylation and Lys 9 and 14 acetylation are increased in dystrophic muscles (7). In addition, disruptions in histone deacetylase (HDAC) activity in dystrophic muscle may contribute to disease severity through dysregulation of epigenetic controls. Pathological increases in HDAC2 activity in *mdx* muscle may lead to reduced expression of the gene encoding follistatin, a protein that is a positive regulator of muscle growth (8), the loss of which may exacerbate muscular dystrophy. Despite the potential importance of these and other perturbations of epigenetic regulation in the pathogenesis of DMD and the demonstrated efficacy of therapeutics designed to normalize the expression or activity of epigenetic regulatory enzymes (9), little is known of the identity of specific genes that experience perturbations of epigenetic regulation during muscular dystrophy.

In this investigation, we explore the possibility that perturbations in the epigenetic regulation of the *klotho* gene affect the pathology of muscular dystrophy. Klotho (KL) is expressed as a transmembrane protein from which the extracellular domain can be cleaved and released to function as a circulating hormone or expressed as a truncated form that is secreted or retained in the cytoplasm (10–12). KL has been studied primarily for its roles in regulating kidney function, where its level of expression is highest (10) and interest has centered on the impact of the progressive loss of KL expression during aging, which contributes to age-related changes in several organs, including kidney and skin (10). KL is also expressed at low levels in skeletal muscle, where its function is unknown (10). However, the reduction of muscle mass and strength in *klotho* hypomorphic mutants (10,13) suggests that it plays a positive, regulatory role influencing muscle function and growth.

The *klotho* gene is under intense epigenetic regulation in several tissues. Kidney tissue exposed to uremic toxins experienced a reduction in KL expression by more than 50% which was associated with increased methylation of the *klotho* promoter region at regions where cytosines are linked to guanine nucleotides by a single phosphate [CpG sites (14)]. Similarly, *klotho* methylation at CpG sites was increased in the kidneys of patients with chronic kidney disease, which was paralleled by decreased KL expression and increased kidney pathology and fibrosis (15). *Klotho* is also highly methylated in tumor tissues, an occurrence that is associated with elevated methylation of CpG sites in the promoter region of *klotho* and *klotho* gene silencing (16–18). In some cancer cell lines, *klotho* silencing can be reversed by reagents that inhibit DNA methyltransferases, especially DNMT1 (DNA methyltransferase-1), that methylate CpG sites (17). Notably, oxidative stress in tissues may drive increases in *klotho* gene methylation and silencing. For example, oxidative stress of cerebellar granule neurons caused reductions in KL expression that were rescued by DNMT inhibitors, which is consistent with the possibility that oxidative stress increases KL methylation at CpG sites, causing gene silencing (19).

Here, we test the hypothesis that *klotho* gene methylation causes gene silencing and worsens the pathology of muscular dystrophy. We also assay for changes in other epigenetic regulatory events, such as histone modifications, that have been associated with *klotho* silencing in other systems (20). We assay for these changes in epigenetic modifications at the time of clinical onset of the disease, which occurs at about 4 weeks of age. This is then followed by a regenerative period, when muscle repair keeps pace with muscle damage. However, at 12 months of age, the mice enter a progressive stage of pathology that eventually leads to their early death (21). We test whether *klotho* gene silencing contributes to any stage of the *mdx* disease progression and assay for the effects of expressing a *klotho* transgene on the pathology of *mdx* dystrophy.

## Results

### Klotho gene expression is silenced after the clinical onset of muscular dystrophy

Quantitative PCR (QPCR) analysis of KL mRNA levels in 2-week-old *mdx* muscles, before clinical onset of the disease, shows that KL expression does not differ from wild-type muscles (Fig. 1A). However, at 4 weeks of age, which is the acute onset of pathology, *klotho* expression in *mdx* muscles is over 80% less than in wild-type muscles. Between 4 and 12 weeks, KL expression declines in both *mdx* and wild-type muscles, although expression remains ~80% lower in *mdx* than in age-matched, 3-month-old wild-type muscles (Fig. 1A and B). Immunohistochemical observations show that in healthy, 3-month-old wild-type muscles that KL expression is detectible in the cytoplasm of muscle fibers, although in age-matched *mdx* muscles KL expression is only observed in mononucleated cells between muscle fibers (Fig. 1C and D). Preabsorbtion of Klotho-specific IgG from the antiserum with recombinant *klotho* depleted all cytosolic staining of wild-type muscle fibers. *Klotho* gene silencing also occurs in DMD muscles after disease onset; biopsies from DMD patients aged 9–17 years old show over an 80% reduction in KL expression compared with healthy, control muscle (Fig. 1E). QPCR data also demonstrate that the reduction of KL expression in *mdx* mice is muscle specific; KL expression is reduced by over 60% in 6-week-old *mdx* muscles compared with controls, but the same mice showed no differences in KL expression in brain, kidney, pancreas or spleen, compared with age-matched control tissues (Fig. 1F).

### *Klotho* gene silencing in *mdx* mice does not affect levels of serum KL

Serum ELISA for circulating levels of KL in 1-month-old mice showed that *mdx* dystrophy did not cause a significant change in serum KL concentrations (wild-type: 977 pg/ml, S.E.M. = 461, $n = 5$; *mdx:* 745 pg/ml, S.E.M. = 108, $n = 6$; $P = 0.61$, two-tailed T-test).

### *Klotho* gene silencing is associated with increased gene methylation in the promoter region and increased dimethylation of H3K9

Because previous investigators have shown that changes in methylation of the *klotho* gene can be important in regulating its expression (14–19,22), we assayed for differences in its methylation that were associated with its silencing in muscular dystrophy. We first assayed for changes in CpG methylation patterns in the promoter region that contains 116 CpGs in a 1420 nt region that borders the transcriptional start site (TSS). We found that there was an increase of over 35% in the methylation levels

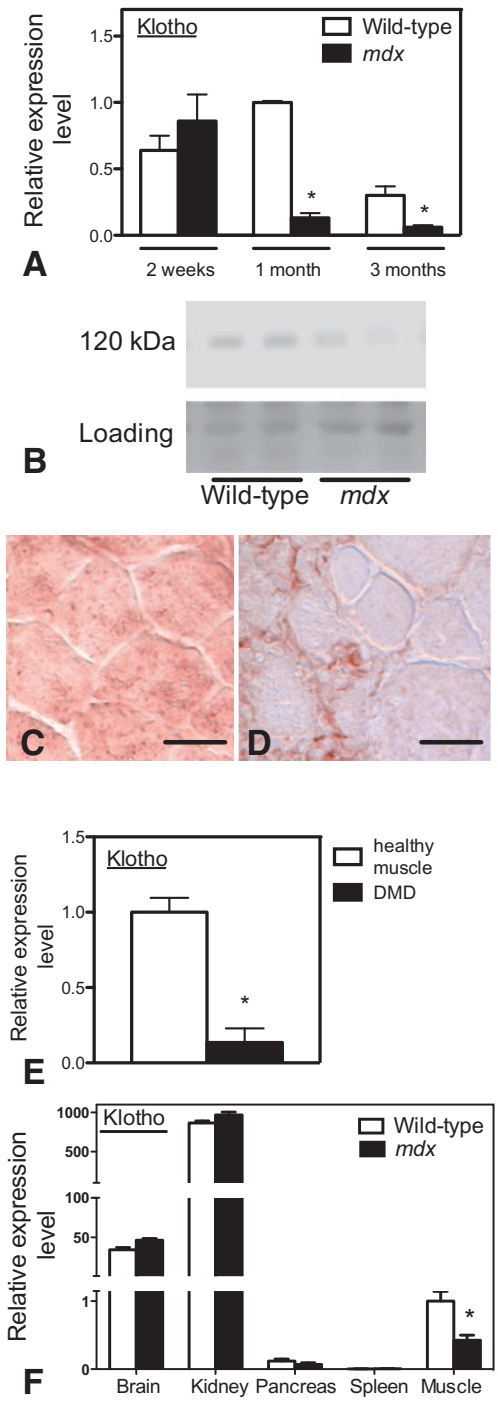


**Figure 1.** *Klotho* expression is selectively silenced in dystrophic muscle at the acute onset of pathology. (**A**) QPCR data showing differences in the level of *klotho* expression in quadriceps muscles of wild-type or dystrophic mice before the onset of pathology (2 weeks) during peak pathology (1 month) or during regeneration (3 months). $N = 5$ for each data set. (**B**) Western blot showing relative expression level of KL in 3-month-old wild-type and *mdx* quadriceps (120 kDa). The same blot was stained with Ponceau Red to show relative loading of the lanes (loading). (**C** and **D**) Cross-sections of 3-month-old wild-type (C) and *mdx* (D) quadriceps muscle labeled with antibodies to KL to show intracellular location in muscle fibers in wild-type muscle. Bars = 30 μm. (**E**) QPCR data showing relative levels of *klotho* expression in muscle biopsies from healthy control boys ($n = 4$) and DMD boys ($n = 3$). * indicates significantly different from control at $P < 0.005$. (**F**) QPCR data showing relative levels of expression of *klotho* in 6-week-old wild-type or *mdx* tissues. $N = 5$ for each data set. * indicates significantly different from control at $P < 0.05$. All data sets analyzed by one-way ANOVA.

of CpG sites in this region of the *klotho* gene (Fig. 2A). We further explored sites at which the *klotho* gene experienced increased methylation associated with its silencing by using R package Biseq to identify regions in which there are consistently and significantly elevated methylation levels. This approach identified a differentially methylated region (DMR) of 119 nucleotides within the 1420 nt region in which the *mdx klotho* gene experienced consistently higher CpG methylation events (Fig. 2B). Furthermore, we performed cluster analysis of methylation levels of *mdx* and wild-type *klotho* genes in the region containing the TSS using the single-clustering method and found that *mdx* and wild-type type data were segregated, indicating two separate populations (Fig. 2C). Finally, we assayed for changes in the expression of enzymes that mediate DNA methylation at CpG sites. We focused on DNMT1 because it is the primary methyltransferase acting on CpG sites in mammals (23) and previous investigators have shown that kidney cells exposed to toxins *in vitro* experience an increase in DNMT1-mediated methylation of *klotho*, leading to a reduction in KL mRNA levels (14). Our findings show that DNMT1 expression is more than two times higher in *mdx* muscles than wild-type muscles at 4 weeks of age, and the elevated levels persist in the muscles of 3-month-old mice (Fig. 2D).

We also found enrichment of H3K9 dimethylation in the *klotho* promoter region in *mdx* muscles. Because previous investigators showed that *mdx* mice experienced global, differential methylation of genes at histone 3 on lysine 79 (H3K79) and lysine 9 (H3K9) and differential acetylation of H3K9 (7), we used chromatin immunoprecipitation (ChIP) assays to test whether the *klotho* gene experienced differential methylation/acetylation at these sites. Although our data show no differences in H3K79 methylation or H3K9 acetylation in *mdx* or wild-type muscles, we found large increases in H3K9 dimethylation on the *klotho* gene in *mdx* muscles using an antibody that was specific for the dimethylated form of K9 on histone 3 (Fig. 2E and F). Because H3K9me2 is a strongly repressive histone mark, the observations indicate that H3K9 dimethylation of *klotho* may play a significant role in its silencing in *mdx* muscle.

## Menadione-induction of H3K9me2 on *klotho* is associated with *klotho* gene silencing

Because increases in oxidative stress can lead to reductions of *klotho* expression in kidney cells *in vitro* (24) and the increase in inflammation in *mdx* muscle at the acute peak of the disease (6) is associated with increased oxidative stress, we assayed whether menadione treatment of muscle cells silenced *klotho* expression *in vitro* (Fig. 3). We observed that treating myotube cultures with menadione, which induces the production of free radicals (25), caused dose–responsive reductions in KL mRNA levels (Fig. 3A). However, menadione treatment did not increase the relative levels of methylation of the promoter region of *klotho*, assessed by methylation specific QPCR (Fig. 3B) despite the increased expression of DNMT1 in menadione-treated cells (Fig. 3D). Furthermore, bisulfite sequencing of the promoter region containing all 116 CpG sites analyzed showed high levels of CpG methylation at all CpG sites throughout the region, including the DMR, in myoblasts and myotubes that were not subjected to menadione treatment (Fig. 3C). In contrast, the same region of *klotho* in DNA isolated from whole muscle tissue showed low levels of CpG methylation (Fig. 3C), indicating that CpG sites are available for methylation and regulation of *klotho* expression in whole muscle *in vivo*, but not muscle cells *in vitro*.

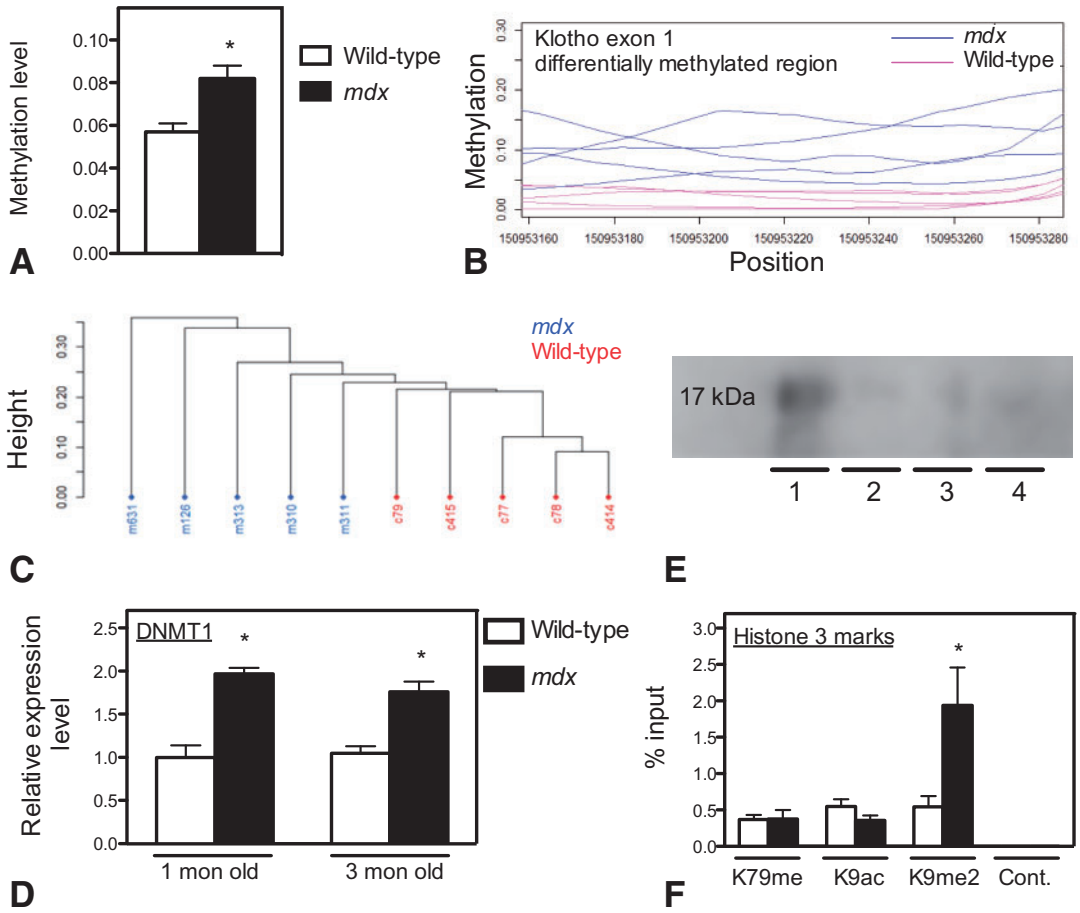


**Figure 2.** *Klotho* experiences increased methylation in *mdx* muscles. (**A**) Bisulfite sequencing data for the 1420 nt region surrounding the TSS of the *klotho* gene in 3-month-old muscle samples shows significant elevation of *klotho* CpG methylation in *mdx* muscles. $N = 5$ for each data set. (**B**) Relative CpG methylation levels within a 119 nt DMR for muscles from 3-month-old *mdx* (blue; $n = 5$) and wild-type (red; $n = 5$) show consistently elevated *klotho* CpG methylation in *mdx* muscles. (**C**) Cluster analysis of CpG methylation levels for the 1420 nt region surrounding the TSS of the *klotho* gene in 3-month-old muscle shows separation of *mdx* and wild-type samples. 'Height' = 0 would represent no differences in CpG methylation between samples; 'height' = 1 would represent all CpG sites differed in methylation status between samples. (**D**) QPCR of DNMT1 expression levels in wild-type ($n = 5$) and *mdx* ($n = 5$) muscles at 1 month and 3 months old shows elevated expression in *mdx* muscles. (**E**) Western blot of H3K9me2 (lane 1), H3 (lane 2), H3K9me1 (lane 3) and H3K9me3 (lane 4) that was probed with antiH3K9me2 that was used in ChIP assays. (**F**) ChIP assay of epigenetic modification of histone 3 at the *klotho* gene showed significant elevations of K9 dimethylation in *mdx* muscles. $N = 5$ for each data set. * indicates significantly different from age-matched control at $P < 0.05$. All data sets analyzed by one-way ANOVA.

We then tested whether histone modifications were associated with *klotho* silencing in muscle cells *in vitro*. ChIP data show that treating myotubes with menadione caused large increases in dimethylation of H3K9 on *klotho*, without affecting H3K79 dimethylation or H3K9 acetylation (Fig. 3E), just as we observed in *mdx* muscle tissue *in vivo*.

## Expression of a *klotho* transgene in *mdx* mice increases longevity and improves function

We assayed whether elevating levels of *klotho* expression in *mdx* mice affected the pathology of *mdx* muscular dystrophy. QPCR and western data confirm that introduction of the *klotho* transgene produced elevations of KL mRNA and protein in *mdx* muscles (KL+/*mdx* mice; Fig. 4A and B). The effect of *klotho* transgene expression on longevity was assayed by recording mortality rate, defined as the percentage of mice in each genotype group that died during the first 2 years of life. During that period, 3.5% of wild-type mice died and 15% of *mdx* mice died (Fig. 4C). However, *klotho* transgene expression in *mdx* mice reduced the proportion of mice dying in the first 2 years to 6.98% (Fig. 4C). In addition, mouse function was improved by transgene expression shown by increases in both the treadmill running time until exhaustion (5.8-fold increase; Fig. 4D) and the wire-hang time (3.4-fold increase; Fig. 4E). *Klotho* transgene expression also caused increases in muscle mass normalized to body mass in *mdx* mice (Fig. 4F–H).

## Expression of a *klotho* transgene in *mdx* mice increases muscle fiber size and number and increases satellite cell number

Histology of muscles from wild-type, *mdx* and KL+/*mdx* mice at 6 months and 2 years shows that *klotho* transgene expression greatly reduces features of *mdx* pathology. During this interval, wild-type muscle shows a progressive reduction in fiber size and increases in interstitial space, attributable to age-related changes (26) (Fig. 5A–I). Over this same period, *mdx* mice show much more loss of fiber size and increases in interstitial space, reflecting the progressive loss of muscle tissue and increased

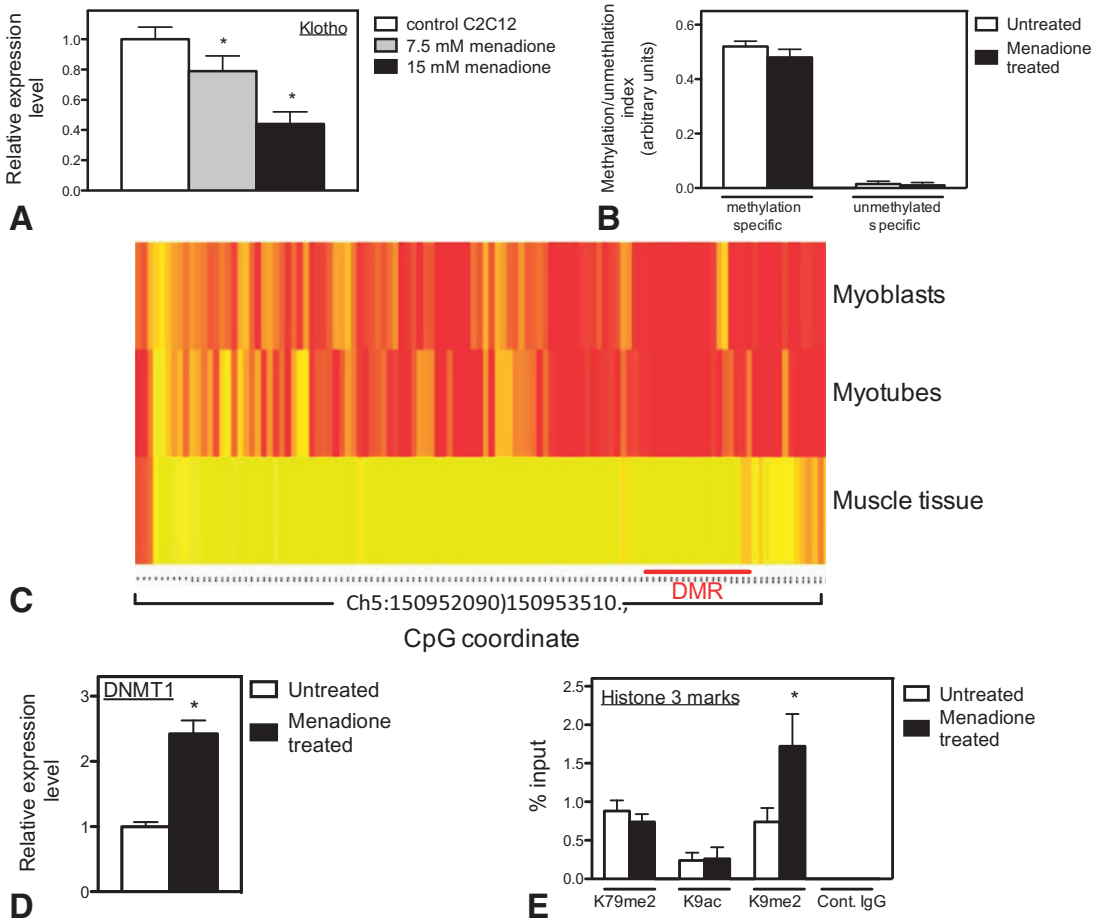


**Figure 3.** Muscle cells *in vitro* exposed to increased oxidative stress show increases in H3K9 dimethylation at the *klotho* gene, but not increased CpG methylation. (**A**) Treatment of myotubes with menadione reduced *klotho* expression. $N = 5$ for each data set. (**B**) Methylation-specific QPCR showed highly elevated levels of *klotho* methylation in myotubes *in vitro* that were not influenced by menadione treatment. $N = 5$ for each data set. (**C**) Heat map for CpG methylation status in the 1420 nt region surrounding the TSS of the *klotho* gene, determined by bisulfite sequencing of myoblasts *in vitro*, myotubes *in vitro* or whole muscle tissue of wild-type mice. Red represents 100% methylation of particular CpG site; yellow indicates 0%. The DMR is indicated by red bar beneath heat map. Note the high level of *klotho* CpG methylation in muscle cells *in vitro*, compared with whole muscle tissue *in vivo*. (**D**) QPCR analysis of myotubes treated with menadione *in vitro* showed increased expression of DNMT1, relative to non-treated myotubes. $N = 5$ for each data set. (**E**) ChIP assay of epigenetic modification of histone 3 at the *klotho* gene showed significant elevations of K9 dimethylation in myotubes subjected to treatment with menadione. $N = 5$ for each data set. * indicates significantly different from age-matched control at $P < 0.05$. All data sets analyzed Student's two-tailed *T*-test.

fibrosis (Fig. 5A–I). However, expression of the *klotho* transgene in *mdx* muscle significantly reduces the loss of fiber size during the late progressive stages of the disease (Fig. 5A–I), especially by increasing the numbers of large diameter fibers (Fig. 5J). This increase in cross-sectional area of the largest fibers in KL+/*mdx* mice results in an increase in variance of fiber cross-section, compared with either wild-type or *mdx* mice (Fig. 5K). *Klotho* transgene expression also prevented the loss of muscle fibers from *mdx* mice as the disease progressed. Although *mdx* mice showed a loss of fiber numbers in muscle cross-sections by more than 50% at 6 months of age, compared with wild-type, fiber numbers for KL+/mdx mice did not differ from wild-type at this age (Fig. 5L). We also observed that *klotho* transgene expression increased Pax7 levels and satellite cell numbers, compared with *mdx*. At 1 month of age, Pax7 expression levels in *mdx* mice were significantly higher than wild-type controls (Fig. 5M), reflecting the activation and expansion of satellite cell populations at the acute onset of the disease. Expression of the *klotho* transgene nearly doubled this expansion (Fig. 5M), which may contribute to improved muscle regeneration. At 6 months of age, Pax7 expression in *mdx* mice was lower than wild-type levels (Fig. 5N), attributable to a depletion of satellite cell populations as the disease progressed. However, expression of the *klotho* transgene in *mdx* mice prevented the reduction of satellite cell populations that occurred in *mdx* mice between 1 month and 6 months of age (Fig. 5N). Counts of the number of satellite cells per muscle fiber in 6-month-old *mdx* and KL+/*mdx* mice (Fig. 5O) showed an insignificant trend for more satellite cells per fiber in mice expressing the *klotho* transgene (Fig. 5P). However, the progressive loss of satellite cells per fiber during the progressive stage of the pathology was prevented by *klotho* transgene expression; in fact, although satellite cell counts in *mdx* mice declined by 60% between 6 and 24 months of age, KL+/*mdx* muscles showed a significant increase of about 42% in satellite cell counts during this same period (Fig. 5P). In contrast, the number of MyoD-expressing cells lying on the surface of muscle fibers increased by 220% in *mdx* muscle between 6 and 24 months of age, but that increase did not occur in KL+/*mdx* muscles (Fig. 5Q).

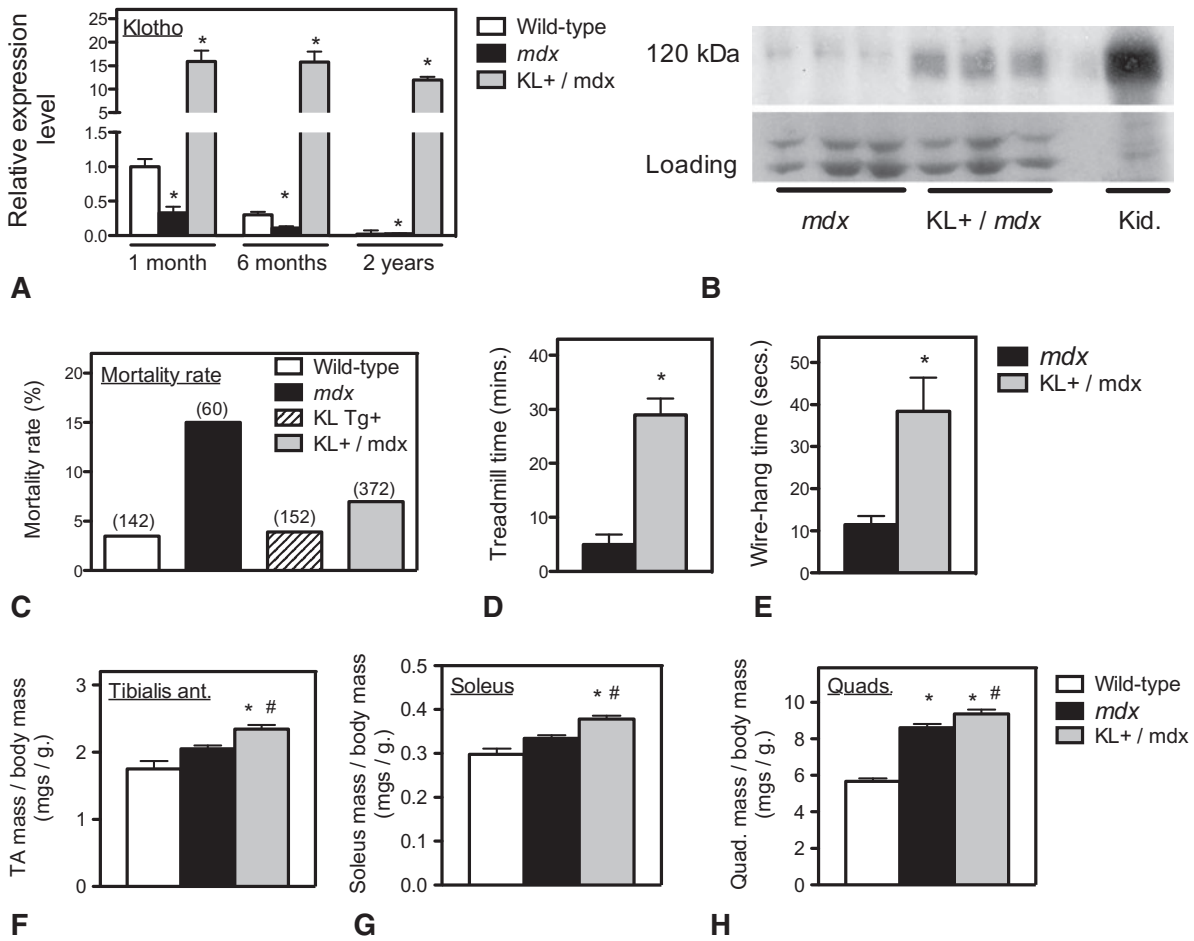


**Figure 4.** Expression of a *klotho* transgene in *mdx* mice increases longevity, function and muscle mass. (**A**) QPCR analysis of *klotho* expression shows a large increase in KL mRNA levels in KL+/*mdx* muscles at all ages, relative to non-transgenic *mdx*. $N = 5$ for each data set. (**B**) Western blot showing relative expression level of KL in 6-month-old *mdx* and KL+/*mdx* quadriceps muscles (120 kDa). The gel was stained with Coomassie Blue dye post-transfer to show relative loading of the lanes (loading). Wild-type mouse kidney extract (Kid.) was used as positive control with the kidney lane loaded with 80% less total protein than muscle extract lanes. (**C**) Expression of a *klotho* transgene in *mdx* mice increases longevity. KL+/*mdx* mortality rate is significantly less than *mdx* and does not differ significantly from wild-type mice. Number of mice in each group is shown parenthetically. Data are the percentage of mice in each genotype group that died during the first 2 years of life. (**D**) Treadmill running time to exhaustion was significantly greater in KL+/*mdx* mice ($n = 11$) than *mdx* mice ($n = 12$). (**E**) Wire-hang time was significantly greater in KL+/*mdx* mice ($n = 13$) than *mdx* mice ($n = 10$). (**F–H**) Expression of a *klotho* transgene in *mdx* mice increased muscle mass relative to body mass compared with *mdx* mice for tibialis anterior (F), soleus (G) and quadriceps (H). $N = 5$ for each data set. * indicates significantly different from age-matched control at $P < 0.05$. # indicates significantly different from age-matched *mdx* at $P < 0.05$. All data sets analyzed by one-way ANOVA.

## Expression of a *klotho* transgene in *mdx* mice does not affect muscle membrane lesions or muscle fiber central nucleation

Histological assays for fiber damage, indicated by cytosolic IgG, or muscle fiber regeneration, indicated by muscle fiber central-nucleation, showed that *mdx* muscular dystrophy increased both pathological features in hind-limb muscles from 6- and 24-month-old mice, compared with wild-type controls. However, expression of the *klotho* transgene had no significant effect on *mdx* muscle fiber damage or central nucleation at either age sampled (Supplementary Material, Fig. 1A and B).

## KL acts directly on muscle cells to increase satellite cell proliferation and increase myotube growth

The large, positive effects of *klotho* transgene expression on retaining muscle mass, fiber size and satellite cell numbers in *mdx* muscular dystrophy suggested that some of the beneficial effects could result from direct actions on muscle cells. We tested this possibility by stimulating wild-type, *mdx* and $C_2C_{12}$ myoblasts *in vitro* with KL in the presence or absence of heparin and FGF23. Heparin enhances KL signaling (27) and KL serves as co-factor for FGF signal activation by FGF23 (28). We found that stimulation of myoblasts with KL together with FGF23 and heparin (KL/FGF23/Hep) more than doubled cell numbers in culture compared with either Hep only, KL/Hep or FGF23/Hep stimulated cultures (Fig. 6A–C). We also found that the increase in cell numbers required the simultaneous stimulation by all three factors (Fig. 6D). We confirmed that the expansion of myoblast numbers was caused by increased proliferation by assaying whether the proportion of proliferative (Ki67+) cells in the cultures was affected by stimulation; KL/FGF23/Hep stimulated cultures showed a nearly 3-fold increase in the proportion of Ki67+ cells compared with Hep only, whereas KL/Hep and FGF23/Hep cultures showed no treatment effect (Fig. 6E). We also confirmed that KL/FGF23/Hep treatment did not influence the proportion of myoblasts that were apoptotic, annexin

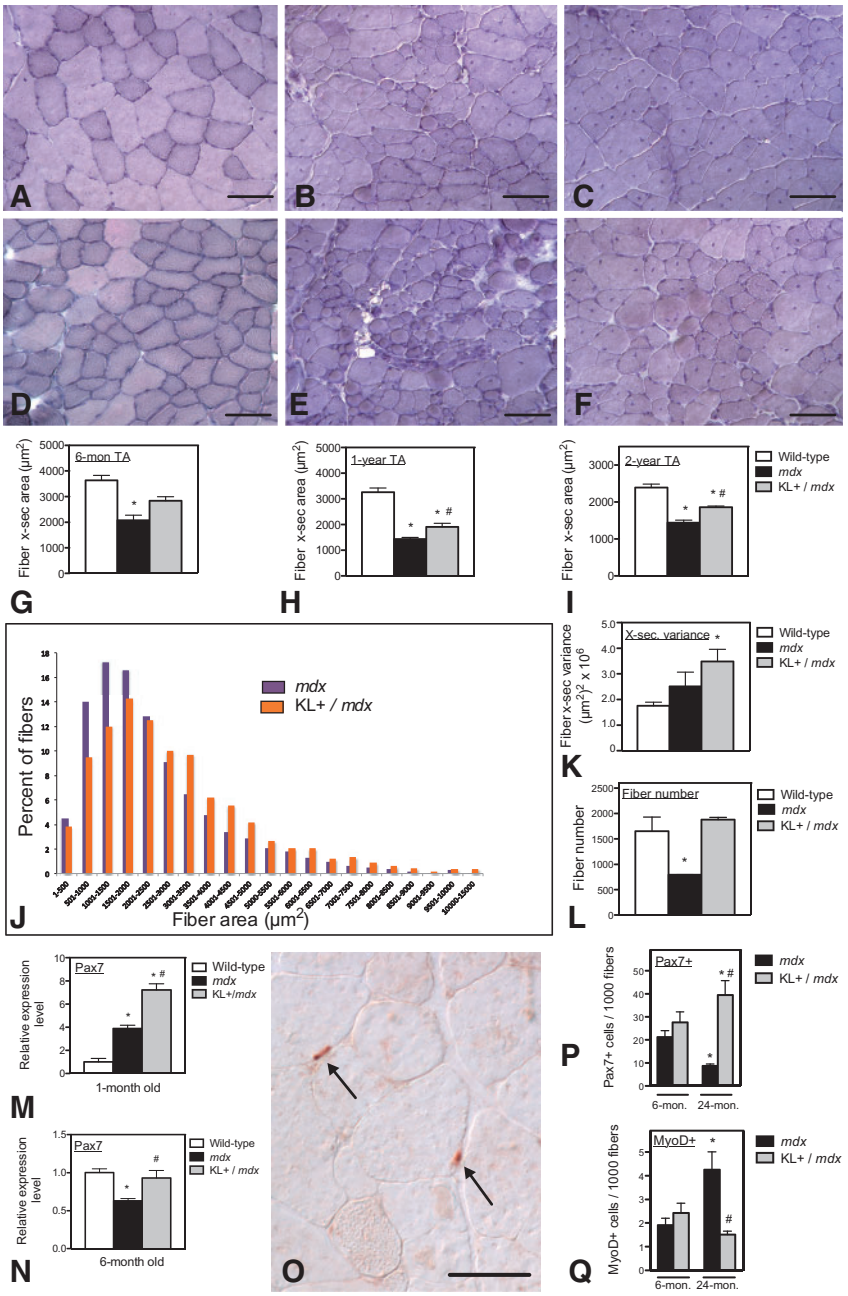


**Figure 5.** Expression of a *klotho* transgene in *mdx* mice reduces histopathology, increases fiber size and number and increases satellite cells per muscle fiber. (**A–F**) Hematoxylin stained cross-sections of tibialis anterior muscles from wild-type (A, D), *mdx* (B, E) and KL+/*mdx* mice (C, F) at 6 months (A–C) and 2 years (D–F) of age. During aging, wild-type mice show a reduction in fiber cross-sectional area, but little accumulation of connective tissue or variability in fiber size (D). At 2 years of age, *mdx* mice show great reductions in fiber size, extensive variability in fiber size and increased space between fibers, reflecting connective tissue accumulation (E). KL+/*mdx* muscle fibers (F) are larger than *mdx* muscle fibers at 2 years and show less connective tissue accumulation. (**G–I**) *Mdx* muscle fiber cross-sectional area is significantly less than wild-type mice at 6 months (G), 1 year (H) and 2 years (I) of age. However, *klotho* transgene expression increases fiber cross-sectional area at 1 and 2 years of age, compared with *mdx*. $N=5$ for each data set. (**J**) Frequency distribution of fiber cross-sectional areas for tibialis anterior muscles from *mdx* (purple bars; $n=5$) and KL+/*mdx* mice (orange bars; $n=5$) shows the shift in fiber sizes to larger cross-sections in transgenic mice. (*K*) Calculation of variance in fiber cross-sectional areas of 6-month-old wild-type, *mdx* and KL+/*mdx* mice shows that transgene expression causes an increase in variability of fiber size, compared with wild-type. $N=5$ for each data set. (**L**) *Mdx* mice show a reduction in the number of muscle fibers per tibialis anterior muscle compared with wild-type muscles that does not occur in KL+/*mdx* mice. $N=5$ for each data set. (**M**) QPCR shows that *mdx* have elevated levels of Pax7 expression at the acute peak of pathology, compared with wild-type, reflecting larger numbers of satellite cells. The Pax7 elevation in KL+/*mdx* mice is even greater at this time point. $N=5$ for each data set. (**N**) At 6 months of age, QPCR analysis shows that *mdx* have reduced levels of Pax7 expression compared with wild-type, reflecting attrition of satellite cell populations. KL+/*mdx* mice do not experience a reduction of Pax7 expression compared with wild-type mice at this time point. For (G–N), * indicates significantly different from age-matched wild-type at $P<0.05$. # indicates significantly different from age-matched *mdx* at $P<0.05$. $N=5$ for each data set. (**O–Q**) Quadriceps muscles of 6-month and 2-year-old *mdx* and KL+/*mdx* mice were immunolabeled for Pax7 (O) or MyoD and the numbers of Pax7+ cells or MyoD+ cells per muscle fiber were assayed (P and Q). Although *mdx* mice experienced a large reduction in satellite cell numbers per fiber over this period (P), satellite cells increased in KL+/*mdx* mice. * indicates significantly different from 6-month-old mice of same genotype at $P<0.05$. # indicates significantly different from age-matched *mdx* at $P<0.05$. $N=5$ for each data set. All data sets analyzed by one-way ANOVA.

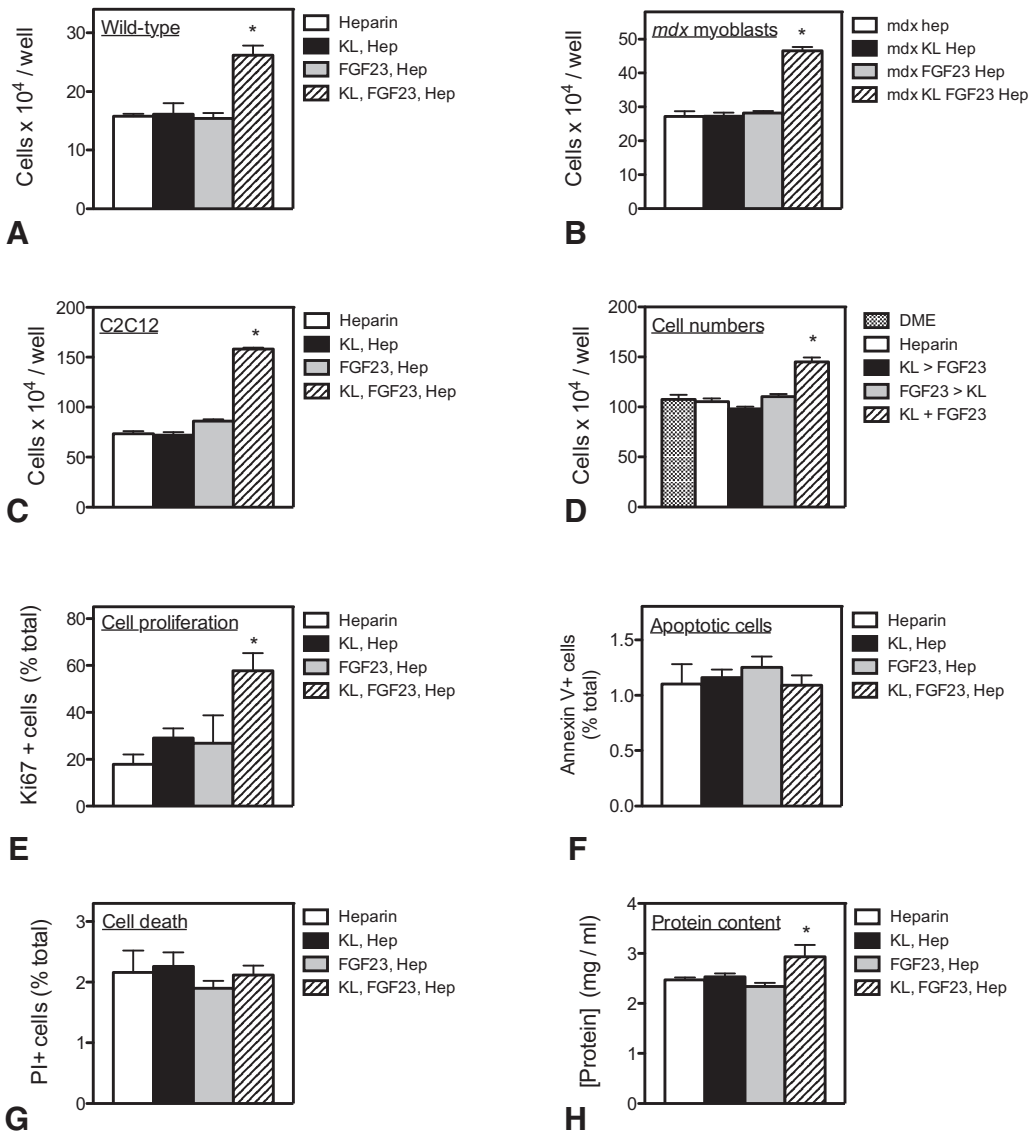


**Figure 6.** KL acts directly on muscle cells to increase their proliferation and to shift toward positive protein balance. (**A–C**) Myoblasts were treated with heparin alone (Hep), KL with heparin (KL, Hep), FGF23 with heparin (FGF23, Hep) or KL with FGF23 and heparin (KL, FGF23, Hep). KL, FGF23, Hep treated cell cultures showed greater increases in cell numbers than all other treatment groups for wild-type primary cultures (A), *mdx* primary cultures (B) and $C_2C_{12}$ cultures (C). (**D**) $C_2C_{12}$ myoblasts were cultured in medium only (DME), medium with heparin (Hep), or stimulated with KL followed by FGF23 (KL > FGF23) or FGF23 followed by KL (FGF23 > KL) or KL and FGF23 together (KL + FGF23). KL + FGF23 treated cultures showed greater increases in cell number than any other treatment group. (**E**) Proportion of myoblasts undergoing cell cycling during the treatment period was assessed by Ki67 labeling. KL, FGF23, Hep cultures were more proliferative than any other treatment group. (**F**) The proportion of myoblasts experiencing apoptosis during the treatment period was assessed by labeling with annexin V. There were no differences in apoptosis between the treatment groups. (**G**) The proportion of myoblasts experiencing necrotic cell death during the treatment period was assessed by labeling with propidium iodide (PI). There were no differences in cell death between the treatment groups. (**H**) Assays for total protein content in $C_2C_{12}$ myotube cultures subjected to different treatment conditions showed that KL, FGF23, Hep treated cultures showed greater accumulations of cellular protein than any other treatment group. $N = 5$ for all data sets. * indicates significantly different from Hep-treated cultures at $P < 0.05$. All data sets analyzed by one-way ANOVA.

V+ (Fig. 6F), or necrotic, propidium iodide+ (Fig. 6G). We also observed positive effects of KL/FGF23/Hep stimulation on post-mitotic myotubes. KL/FGF23/Hep stimulation increased the protein content of myotube cultures, indicating a shift toward a positive protein balance (Fig. 6H).

### *Klotho* transgene expression reduces *mdx* muscle fibrosis during late, progressive stages of the pathology

The histological observations that *klotho* transgene expression decreased the interstitial space between *mdx* muscle fibers during the progressive stages of *mdx* pathology suggested that KL may inhibit fibrosis during this stage of the disease. We tested this possibility by assaying for the effects of transgene expression on two major connective tissue proteins that contribute to *mdx* pathology, collagen types 1 and 3. QPCR data show that expression levels of both collagens are elevated in the early acute-onset and regenerative stages of the disease, but expression of the *klotho* transgene has no effects on collagen expression at these stages (Fig. 7A–F). However, during the late, progressive stage of pathology at 24 months old, the large increases in expression of both collagens in *mdx* muscle compared with controls are reduced by approximately half by *klotho*

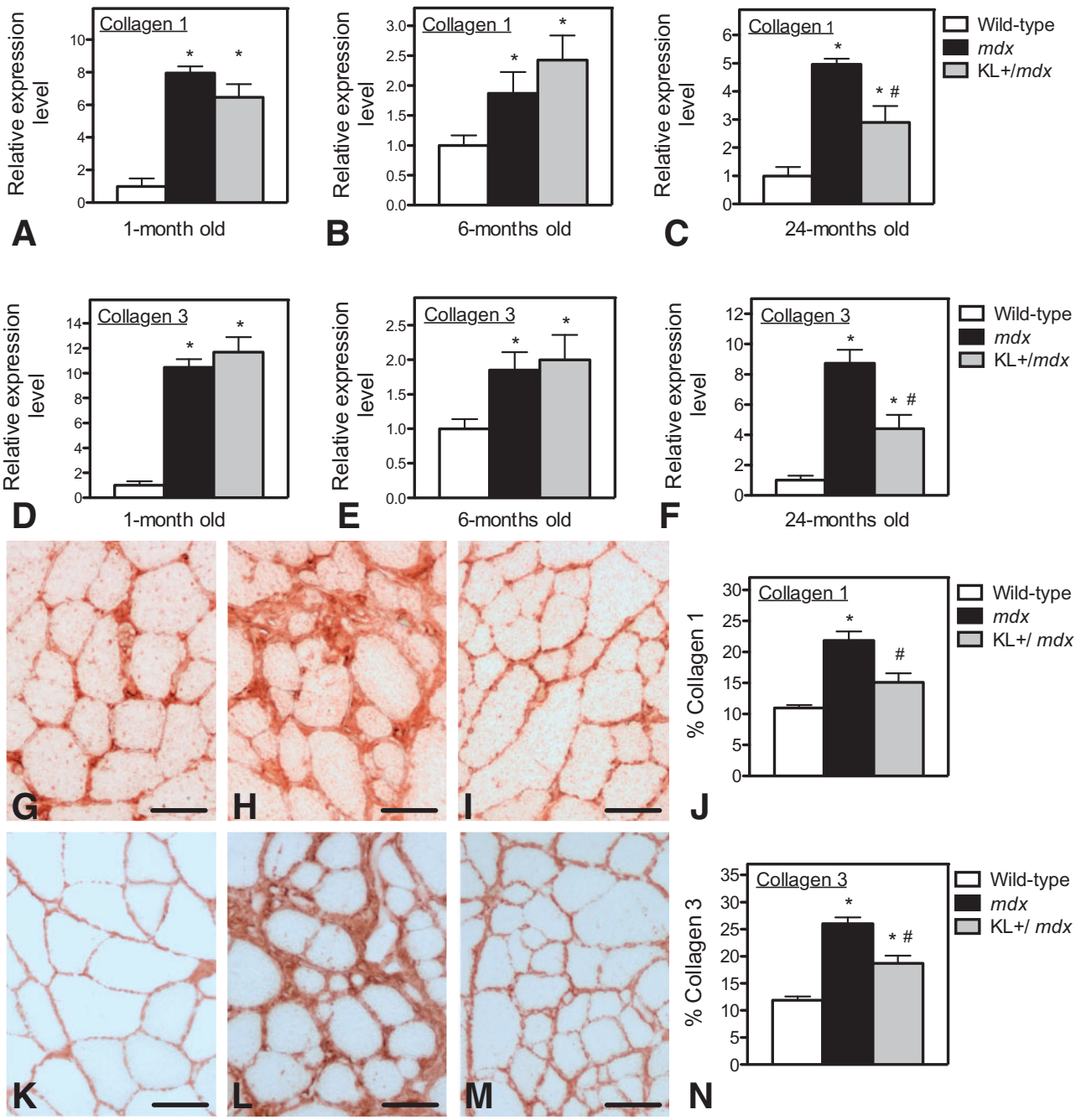


**Figure 7.** *Klotho* transgene expression reduces fibrosis of dystrophic muscles during progressive stages of the pathology. QPCR analysis of quadriceps muscle shows elevated levels of expression of collagen type 1 (**A–C**) and collagen type 3 (**D–F**) at 1 month (A, D), 6 months (B, E) and 24 months (C, F) of age. Although expression of the *klotho* transgene in *mdx* mice does not affect collagen expression in *mdx* mice at 1 or 6 months, transgene expression causes a large, significant reduction in the expression of collagen types 1 and 3 at 24 months (C, F). Immunohistochemistry of collagen type 1 accumulation in 24-month-old muscles from wild-type (**G**), *mdx* (**H**) or KL+/*mdx* mice (**I**) shows that the volume fraction of muscle that is occupied by collagen type 1 is significantly increased in *mdx* mice compared with wild-type (**J**). However, there is no significant increase in KL+/*mdx* muscles compared with wild-type (J). Immunohistochemistry of collagen type 3 accumulation in 24-month-old muscles from quadriceps muscles of wild-type (**K**), *mdx* (**L**) or KL+/*mdx* mice (**M**) shows that the volume fraction of muscle that is occupied by collagen type 3 is also significantly increased in *mdx* mice compared with wild-type (**N**). Expression of the *klotho* transgene significantly reduces collagen type 3 accumulation in *mdx* muscles. $N = 5$ for each data set. * indicates significantly different from age-matched wild-type at $P < 0.05$. # indicates significantly different from age-matched *mdx* at $P < 0.05$. All data sets analyzed by one-way ANOVA.

transgene expression (collagen type 1, 52% reduction; collagen type 3, 56% reduction; Fig. 7C and F). These effects on expression are also reflected in the accumulation of the collagens in the interstitial space of 24-month-old muscles (Fig. 7G–N). Although the proportion of *mdx* muscle that was occupied by collagen type 1 increased 100% in 24-month-old mice, that increase was reduced by 54% by *klotho* transgene expression (Fig. 7G–J). Similarly, the 119% increase in collagen type 3 in 24-month-old *mdx* muscles was reduced by 49% by transgene expression (Fig. 7K–N).

### *Klotho* transgene expression shows age-dependent effects on profibrotic signaling pathways

Fibrosis of muscle during muscular dystrophy and aging can be promoted by at least three pathways that likely overlap. A switch in satellite cell phenotype from a myogenic to a fibrogenic phenotype that requires increased expression in axin-2 and is promoted by TGFβ has been implicated in muscle fibrosis during aging and muscular dystrophy (29,30). Increased expression of TGFβ has been associated with increased muscle fibrosis by elevating numbers and activities of fibroblasts and fibro-adipogenic precursor cells (31,32) and elevated expression of arginase contributes significantly to increased fibrosis in both aging and dystrophic muscle (33,34). We tested whether *klotho* transgene expression affected the expression of key transcripts in these pro-fibrotic mechanisms by assaying expression levels of axin-2, TGF-β1 and arginase-1 in 1- and 24-month-old *mdx* muscles. We found that at 1 month of age, there was a 3- to 6-fold increase in each of the transcripts assayed in *mdx* muscles compared with controls (Fig. 8A–C). However, *klotho* transgene expression had no effect on axin-2 or arginase expression, and produced only a small reduction in TGF-β1 expression. In 24-month-old muscles, TGF-β1 and arginase expression in *mdx* muscles were again elevated 2- to 6-fold, although there was no increase in axin-2 expression compared with wild-type muscles (Fig. 8D–F). In these late stages of the pathology, *klotho* transgene expression again had no significant effect on arginase expression and produced a small reduction in axin-2 expression. However, KL+/*mdx* mice showed a 51% reduction of TGF-β1 expression compared with *mdx* muscles at 24 months of age, suggesting that KL may reduce fibrosis of dystrophic muscle during late progressive stages of the disease through reductions of TGFβ signaling (Fig. 8E).

## Discussion

The current investigation indicates that epigenetic silencing of the *klotho* gene is an important feature of pathogenesis in the *mdx* model of DMD. Our findings show that after the acute onset of pathology in *mdx* muscles, *klotho* undergoes increased methylation of CpG sites in the promoter region of the gene, which is associated with gene silencing. There is also a significant increase in a repressive histone mark, dimethylated H3K9, on the *klotho* gene, which also contributes to gene silencing. This increased dimethylation of H3K9 on *klotho* is contrary to the reported reduction in *mdx* myonuclei that stain positively for H3K9me2 (7), indicating that there is some selectivity for the *klotho* H3K9 dimethylation in muscular dystrophy. We have also learned that expression of a *klotho* transgene restores longevity of *mdx* mice to wild-type levels, reduces wasting of muscle fibers during progressive stages of *mdx* pathology, improves muscle function and greatly increases the satellite cell pool, even at late stages of the disease. Thus, manipulation of *klotho* expression through either the pathological dysregulation of epigenetic controls or experimental perturbations of gene expression *in vivo* can have broad, significant effects on the severity of muscular dystrophy.

We were interested to learn that the silencing of the *klotho* gene occurs selectively in muscles of *mdx* mice and that this tissue-specific effect is sufficient to promote pathology substantially. The increase in pathology occurs despite the more than 2000 times higher level of expression of *klotho* in *mdx* kidneys and more than 100-fold higher expression in *mdx* brains, in which *klotho* expression is not affected by dystrophin deficiency. This suggests that KL-mediated effects on muscle homeostasis are largely paracrine and that KL's endocrine effects in *mdx* muscular dystrophy are not sufficient to rescue muscle from muscle-specific silencing of the *klotho* gene. Although full-length KL is a type 1 transmembrane protein over 1000 amino acids long, the intracellular domain is only 10 amino acids and the large extracellular domain can be cleaved for its release into the circulation to function as a hormone (35). However, another KL transcript that is generated through alternative transcriptional termination encodes a protein that is retained in the cytosol until it is released to act as a humoral factor (36). Our finding that muscle KL is detectible in the cytoplasm but not at the cell surface suggests that KL derived from the cytosolic compartment contributes to maintaining muscle homeostasis, although it is also possible that functional KL is released rapidly from the sarcolemma, before accumulating to levels detectible by immunohistochemistry.

Our *in vivo* data showing that *klotho* silencing was associated with increases in *klotho* CpG methylation in the region of the TSS agree with the findings of other investigators concerning *klotho* silencing in kidney, cancer cells and neurons (14–19), but our *in vitro* data did not show an association between *klotho* silencing and CpG methylation. Despite the reduction of *klotho* expression and the increase in DNMT1 expression in menadione-treated muscle cells *in vitro*, no significant change in CpG methylation occurred. This finding reflects, in part, the high level of *klotho* methylation that occurs in unstressed muscle cells *in vitro* so that further increases in methylation may be difficult to resolve. The results also suggest that *klotho* silencing in menadione-treated muscle cells *in vitro* may occur primarily through other mechanisms, such as H3K9 dimethylation. Although whether the increased dimethylation of H3K9 is specifically a consequence of oxidative stress or some other menadione-mediated stress remains to be explored, the menadione treatment provided a mechanism to increase *klotho* H3K9 dimethylation *in vitro*, which produced *klotho* gene silencing. This parallels the increase in H3K9 dimethylation of *klotho* in *mdx* muscle *in vivo* that is associated with *klotho* gene silencing, which supports the interpretation that H3K9 methylation status is important in influencing *klotho* expression in muscle.

Our findings indicate that the loss of the normal renewal capacity of satellite cells is a primary defect in muscular dystrophy that is exacerbated by *klotho* gene silencing. Our observations show that KL is a strong mitogen that can cause a doubling of myoblast numbers *in vitro* within 48 h compared with non-stimulated control myoblasts. This is consistent with the *in vivo* effects of expression of the *klotho* transgene, in which the loss of satellite cells at progressive stages of the disease was prevented. Although it is controversial whether loss of satellite cells is a primary factor in muscle wasting that occurs in normal aging (37), loss of the renewal capacity of satellite cells is expected to be a significant feature of DMD and *mdx* pathology during the progressive stage (38). KL-mediated increases in satellite cell renewal may be sufficient to explain how the *klotho* transgene increases muscle mass and muscle fiber size in *mdx* mice, but our *in vitro* observations also show that KL treatment of post-mitotic myotubes increases protein content. This indicates that increases in muscle fiber size in KL+/*mdx* mice may also reflect an additional mechanism through which KL shifts multinucleated muscle cells to a more positive protein balance.

Despite our data showing that *klotho* transgene expression in *mdx* mice restored them to the longevity of wild-type mice, we cannot conclude that the increased longevity was caused by beneficial effects of the transgene on the dystrophic pathology,

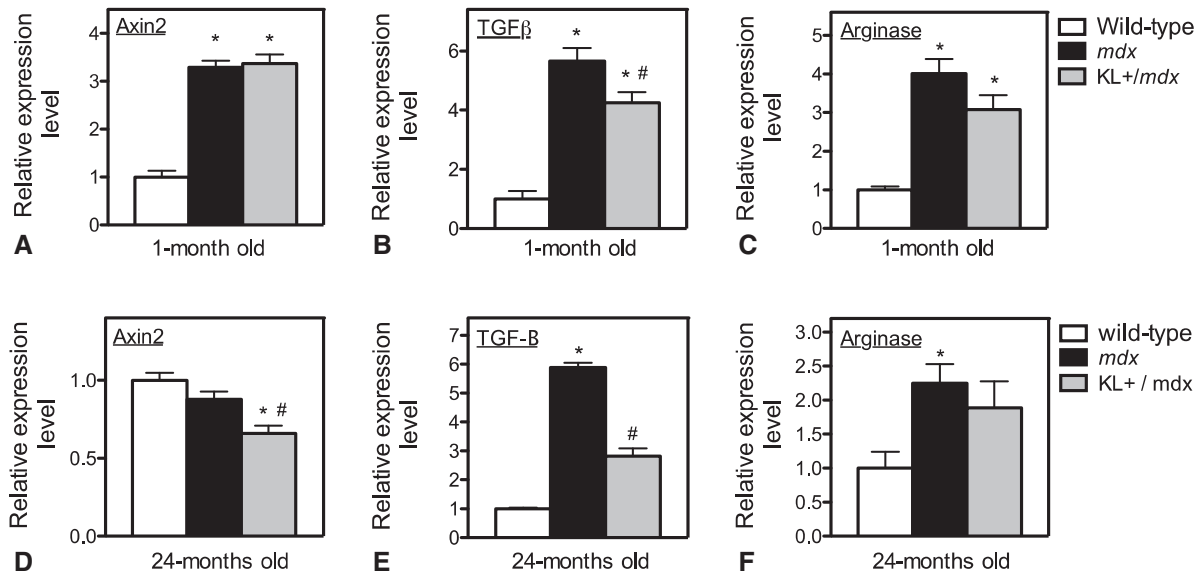


**Figure 8.** *Klotho* transgene expression reduces the expression of transcripts associated with the Wnt/TGFβ profibrotic axis in the late, progressive stages of *mdx* dystrophy. QPCR analysis shows elevation of transcripts associated with profibrotic processes in dystrophic muscle are elevated at the acute peak of *mdx* pathology (1 month old) (**A–C**), but expression of the *klotho* transgene causes only a small reduction in expression of TGFβ1 at this stage of the disease. At the late progressive stage of pathology (24 months old), *klotho* transgene expression reduces expression of axin-2 (**D**) and TGFβ1 (**E**), but does not affect arginase-1 expression (**F**). $N = 5$ for each data set. * indicates significantly different from age-matched wild-type at $P < 0.05$. # indicates significantly different from age-matched *mdx* at $P < 0.05$. All data sets analyzed by one-way ANOVA.

*per se*. Expression of the *klotho* transgene on the wild-type background caused a 20–30% increase of lifespan, attributable to compensation for the systemic loss of *klotho* expression in multiple tissue that occurs during normal aging (28). Nevertheless, whether improvement in *mdx* mouse longevity by the *klotho* transgene compensated or corrected the defect reducing lifespan, the findings support the possibility that increased KL delivery to dystrophin-deficient individuals can provide a mechanism to increase their longevity.

The large reduction of muscle fibrosis that occurred during the progressive stage of *mdx* pathology was a strong, beneficial effect of elevated KL production. This outcome is important in the context of KL's potential therapeutic value in DMD because muscle fibrosis is a particularly morbid condition in DMD that can negatively affect mobility, respiration and cardiac function. Previous investigators have established that reductions in *klotho* expression contribute to increased renal fibrosis caused by unilateral urethral obstruction [UUO (39)]. Furthermore, treatment with recombinant KL or expression of a *klotho* transgene reduced renal fibrosis caused by UUO (40,41) and delivery of a *klotho* construct by adeno-associated virus reduced vascular fibrosis in a rodent model of atherosclerosis (42). The antifibrotic effect of KL in muscular dystrophy and renal fibrosis may function through inhibition of similar pro-fibrotic pathways. Elevations in the expression or activity TGF-β1 are associated with increased tissue fibrosis in muscular dystrophy and renal fibrosis (39,40,43). Increases in KL delivery to dystrophic muscle or fibrotic kidneys cause large reductions in TGF-β1 expression (present investigation; 39,41,44) and corresponding reductions in the expression of collagen genes (present investigation; 41). Activation of TGFβ-mediated fibrosis in dystrophic muscle and fibrotic kidneys is driven partially by increased signaling through the Wnt pathway (30,42). KL binds directly to Wnt leading to inhibition of Wnt signaling and reductions in TGF-β1 expression (41,45). In the present investigation, we assessed increases in axin-2 expression as an index of increased Wnt signaling because axin-2 is a target gene of Wnt and elevations of axin-2 mRNA in muscle reflect elevations in Wnt signaling (29). Our observation that elevations of *klotho* expression in fibrotic, 2-year-old *mdx* muscle produce reductions in axin-2 and TGF-β1 expression that correspond to lower levels of collagen type 1 and type 3 expression and less fibrosis implicates the Wnt–TGFβ–collagen pathway as a target for KL-mediated inhibition of fibrosis in muscular dystrophy. However, we found no effect of *klotho* transgene expression on the increase in arginase expression in *mdx* muscles although increases in arginase expression by intramuscular macrophages significantly increase muscle fibrosis in *mdx* mice and in aging muscles (33,34).

Although the identity of the specific cell types in dystrophic muscle that are influenced by the loss of KL expression to become pro-fibrotic is unknown, activation of either fibroblasts or satellite cells by TGFβ can increase their expression of fibrotic genes, especially those encoding the collagens (46,47). Satellite cells in aging muscle undergo a shift to a more fibrotic, less myogenic phenotype that is attributable to activation of canonical Wnt signaling in satellite cells and associated with a reduction in muscle fiber size and increased production of connective tissue (29). Because KL is a negative regulator of Wnt signaling, loss of muscle KL in *mdx* mice could contribute to a shift of satellite cells to a more fibrotic phenotype. However, TGFβ also activates a population of fibrogenic cells in muscle that express platelet-derived growth factor receptor-alpha (PDGFRα). These cells, called PDGFRα+ mesenchymal progenitors (48) or fibro/adipogenic progenitors [FAPs (49)] are also activated to a more fibrogenic phenotype by TGFβ, although whether this is mediated by Wnt signaling is unknown.

We believe that a particularly useful aspect of our work is that we have associated epigenetic silencing of a specific gene, *klotho*, with two major features of the pathology of *mdx* muscular dystrophy: the progressive loss of satellite cells and the accumulation of fibrotic material. Those findings suggest that KL-based therapeutics could provide multiple benefits for the

treatment of muscular dystrophy. However, a perplexing finding that could become an obstacle for using KL delivery to treat muscular dystrophy is that skeletal muscle is a minor contributor to systemic KL, although its muscle-specific silencing contributes greatly to aspects of the pathology that we identify in our study. That observation tells us that the beneficial effects of KL expression on skeletal muscle health are more likely mediated through autocrine or paracrine effects, and perhaps pharmacological elevations of systemic KL will not provide rescue from features of the dystrophic pathology. Continuing studies are designed to test this question.

## Materials and Methods

### Human tissues

Human muscle samples were obtained from archived frozen skeletal muscle tissue removed for diagnostic purposes, with no pending clinicopathologic testing and for which a diagnosis of muscular dystrophy was rendered. Tissue samples were provided without patient identifiers according to guidelines approved by the UCLA Institutional Review Board.

### Mice

All animals were handled according to guidelines approved by the Chancellor's Animal Research committee at the University of California, Los Angeles. C57BL/6 (wild-type mice) and C57BL/10ScSn-Dmd$^{mdx}$/J mice (*mdx* mice) were purchased from The Jackson Laboratory (Bar Harbor, ME) and bred in pathogen-free vivaria at the University of California, Los Angeles. The generation of transgenic mice that overexpress *klotho* (EFmKL46) has been described previously (10). The transgene is under control of the elongation factor 1α promoter that causes systemic expression of the transcript. Mice carrying the *klotho* transgene were crossed into the C57BL/6 background for a minimum of six generations and then crossed into the *mdx* background using a previously described breeding strategy (6,50). Expression of the *klotho* transgene was confirmed by QPCR and western blot. Null mutation of the dystrophin gene was confirmed using *mdx*-amplification-resistant mutation system PCR (51). Primers are listed in Table 1.

### RNA isolation and qPCR

Muscles were homogenized in Trizol (Invitrogen) and RNA was extracted, isolated and DNase-treated using RNeasy spin

**Table 1.** Primers used in the investigation

| Gene | Accession number | | Direction (5′→3′) | Amplicon size (bp) |
|---|---|---|---|---|
| Arg1 | NM_007482 | Fwd | CAATGAAGAGCTGGCTGGTGT | 153 |
| | | Rev | GTGTGAGCATCCACCCAAATG | |
| Axin2 | NM_015732.4 | Fwd | GACGCACTGACCGACGATTC | 107 |
| | | Rev | CTGCGATGCATCTCTCTCTGG | |
| Col I | NM_007742.3 | Fwd | TGTGTGCGATGACGTGCAAT | 133 |
| | | Rev | GGGTCCCTCGACTCCTACA | |
| Col III | NM_009930.2 | Fwd | ATCCCATTTGGAGAATGTTGTGC | 200 |
| | | Rev | GGACATGATTCACAGATTCCAGG | |
| CD163 | NM_053094.2 | Fwd | GCAAAAACTGGCAGTGGG | 164 |
| | | Rev | GTCAAAATCACAGACGGAGC | |
| DNMT1 | NM_010066.4 | Fwd | ATCCTGTGAACGAGACCCTGT | 96 |
| | | Rev | CCGATGCGATAGGGCTCTG | |
| Klotho | NM_013823.2 | Fwd | GTCTCGGGAACCACCAAAAG | 150 |
| | | Rev | CTATGCCACTCGAAACCGTC | |
| hKlotho | NM_004795.3 | Fwd | CCAATGGAATCGATGACGGG | 153 |
| | | Rev | GAGCTGTGCGGTCGTTAAAC | |
| Pax7 | NM_011039.2 | Fwd | CTCAGTGAGTTCGATTAGCCG | 144 |
| | | Rev | AGACGGTTCCCTTTGTCGC | |
| TGFb1 | NM_011577.1 | Fwd | CTCCACCTGCAAGACCAT | 84 |
| | | Rev | CTTAGTTTGGACAGGATCTGG | |
| RNPS1 | NM_001080127.1 | Fwd | AGGCTCACCAGGAATGTGAC | 196 |
| | | Rev | CTTGGCCATCAATTTGTCCT | |
| SRP14 | NM_009273.4 | Fwd | GAGAGCGAGCAGTTCCTGAC | 196 |
| | | Rev | CGGTGCTGATCTTCCTTTTC | |
| hEEF1A1 | NM_001402.5 | Fwd | CTTTGGGTCGCTTTGCTGTT | 183 |
| | | Rev | CCGTTCTTCCACCACTGATT | |
| hPPIA | NM_021130.4 | Fwd | GCAGACAAGGTCCCAAAGAC | 121 |
| | | Rev | CACCACCCTGACACATAAACC | |
| Klotho Methylation (MSP) | NC_000071.6 | Fwd | CGTTGTTTGAGCGTTGAGTC | 110 |
| | | Rev | AAACCGTCGAAAAAAATATCGTA | |
| Klotho Unmethylation (MSP) | NC_000071.6 | Fwd | TTTGTTGTTTGAGTGTTGAGTTG | 114 |
| | | Rev | AAAAACCATCAAAAAAAATATCATA | |
| Input control (MSP) | NC_000071.6 | Fwd | TAGTTTTAGGAAGGTAAAGGGAGTG | 172 |
| | | Rev | AAATACCCAAAAAAAACACAACAAA | |
| Klotho ChIP | NC_000071.6 | Fwd | AAACCTCGCAAAGTTCCACC | 199 |
| | | Rev | CAGAAACAGCTGCCCAACTT | |

columns according the manufacturer's protocol (Qiagen). RNA was then electrophoresed on agarose gels and RNA quality assessed by 28S and 18S ribosomal RNA integrity. RNA was reverse transcribed with Super Script Reverse Transcriptase II using oligo dTs to prime extension (Invitrogen). The cDNA was then used to assay the expression of selected transcripts using SYBR green QPCR Supermix according to the manufacturer's protocol (BioRad). Real-time PCR was performed on an iCycler thermocycler system equipped with iQ5 optical system software (BioRad). We used established guidelines for sample preparation, experimental design, data normalization and data analysis for QPCR to maximize the rigor of quantifying the relative levels of mRNA (52,53). We also empirically identified reference genes that did not vary between our experimental groups (RNPS1 and SRP14) using geNorm 3.5 software, as described previously (54). The normalization factor for each sample was calculated by geometric averaging of the Ct values of reference genes using the geNorm software. The expression for each gene in control samples was set to 1 and the other expression values were then scaled to that value. Primers used for QPCR are listed in Table 1.

## Western blots

The expression levels of KL in muscles were assayed by western blot analysis. Equal loading of samples was confirmed by staining nitrocellulose blots with 0.1% Ponceau S solution (Sigma-Aldrich). Nitrocellulose membranes were blocked with 50 mM sodium phosphate buffer pH 7.4 containing 200 mM sodium chloride (phosphate-buffered saline; PBS) and containing 0.1% Tween-20 and 3% non-fat dried milk. The membranes were probed with rabbit anti-mouse KL (Abcam #75023) for 3 h at room temperature. Membranes were then washed with PBS containing 0.05% Tween-20 and probed with horseradish peroxidase (HRP) conjugated-donkey anti-rabbit IgG (Amersham, 1:10 000) for 1 h at room temperature. Membranes were washed and the expression levels of KL were visualized with chemiluminescent substrate and a fluorochem imaging system (Alpha Innotech).

The specificity of the antibody to the dimethylated H3K9 (Abcam) that was used for ChIP assays was also tested by western blot. Lanes of gels were loaded with 2 μg of histone 3 (H3), H3K9me1, H3K9me2 or H3K9me3 (Abcam), electrophoresed, transferred to nitrocellulose membrane and then probed with mouse anti-H3K9me2. The blots were then washed and incubated with HRP-conjugated anti-mouse IgG before imaging using chemifluorescence.

## ELISA

Whole blood was collected from the femoral artery and allowed to clot on ice for at least 30 min. The whole blood was spun for 10 min at 2000 rpm at 4°C. The supernatant was collected and stored in liquid nitrogen until analyzed by ELISA using a mouse *klotho* ELISA kit (Cloud Clone Corp.) Samples were thawed and placed in a microwell plate coated with an anti-mouse KL antibody according to the manufacturer's instructions. Following an HRP-based reaction, a colored product was formed in proportion to the amount of KL present, which was analyzed by a spectrophotometer (Bio-Rad Benchmark Microplate Reader) at a wavelength of 450 nm. The concentration of KL was determined by comparing the optical density of the samples to the standard curve.

## Immunohistochemistry

Muscles were dissected from euthanized mice and then rapidly frozen in liquid nitrogen-cooled isopentane. Cross-sections of 10 μm thick were taken from the mid-belly of muscles, air-dried for 30 min and then fixed in ice-cold acetone for 10 min. Sections were blocked for 1 h with 3% bovine serum albumin (BSA) and 0.05% Tween-20 diluted in 50 mM Tris–HCl pH 7.6 containing 150 mM NaCl. Sections were then incubated overnight at 4°C with rabbit anti-mouse KL, or rabbit anti-collagen type 1 (1:50; Chemicon International) or goat anti-collagen 3 (1:50; Southern Biotech). The sections were washed with PBS and probed with biotin-conjugated secondary antibodies (Vector Laboratories, 1:200) for 1 h at room temperature. Sections were subsequently washed with PBS and then incubated for 30 min with avidin D-conjugated HRP (Vector, 1:1000). Staining was visualized with the peroxidase substrate, 3-amino-9-ethylcarbazole (Vector), yielding a red reaction product. Sections labeled with rabbit anti-MyoD (Santa Cruz, 1:50) were processed identically, except they were fixed with 2% paraformaldehyde. For negative control preparations for anti-KL labeling, the antiserum was mixed overnight at 4°C with 10 μg of recombinant, full-length KL (Abcam) per ml of antiserum diluted at 1:50 in 50 mM Tris–HCl pH 7.6 containing 150 mM NaCl. Antibody complexed with antigen was centrifuged from the mixture at 10 000*g* for 10 min and the supernatant devoid of anti-KL IgG was used for labeling sections.

## Production of Pax7 antibody and immunohistochemistry

Pax7 hybridoma cells were purchased from Developmental Studies Hybridoma Bank (Iowa City Iowa). Cells were cultured in complete medium consisting of Dulbecco's Modified Eagle Medium (DMEM) with 1% penicillin–streptomycin (Gibco) and 20% heat-inactivated fetal bovine serum (FBS). Conditioned medium was collected 48 h later and centrifuged at 400*g* for 3 min. The supernatant was applied to an affinity chromatography column containing anti-mouse IgG-agarose beads (Sigma-Aldrich). Unbound protein was washed from the column and bound protein was then fractionated in glycine buffer containing 100 mM glycine (ACROS Organics) at pH 2.2. Protein concentration of each fraction was determined by measuring absorbance at 280 nm. Specificity of the antibody was tested by western blotting with the antibody only or antibody pre-incubated with Pax7 blocking peptide (Aviva Systems Biology). The antibody was then used for anti-Pax7 labeling of frozen muscle cross-sections. Sections were air-dried for 30 min and fixed in 2% paraformaldedye for 10 min. Sections were then immersed in antigen retrieval buffer (10 mM sodium citrate, 0.05% Tween 20, pH 6.0) at 95–100°C for 40 min. Endogenous peroxidase activity in the tissue was quenched by immersion in 0.3% $H_2O_2$. Sections were then treated with blocking buffer from a mouse-on-mouse immunohistochemistry kit (M.O.M kit; Vector) for 1 h and immunolabeled with affinity purified mouse anti-Pax7 antibody overnight at 4°C. Sections were washed with PBS and then incubated with biotin-conjugated anti-mouse IgG (1:250) for 30 min. Sections were subsequently washed with PBS and then incubated for 30 min with ABC reagents from the M.O.M kit. Staining was visualized with the peroxidase substrate 3-amino-9-ethylcarbazole (AEC kit; Vector), yielding a red reaction product.

## Satellite cell counts

The number of satellite cells/sectioned muscle fiber was determined by counting the number of Pax7+ cells in mid-belly

cross-sections of muscles and the total number of fibers per cross-section.

### Methylation-specific PCR

Hamstring or quadriceps muscles (100 mg) were lysed in 750 μl Tris–EDTA buffer with 100 μl Protease K at 55 °C for 48 h. Genomic DNA samples were then purified by phenol–chloroform extraction. Genomic DNA samples were subjected to bisulfite conversion in which all the non-methylated cytosine residues were converted into uracil via deamination, whereas methylated cytosine remained unreacted. Bisulfite treated DNA (300 ng) was used for real-time PCR analysis using methylation and unmethylated specific primers. The methylation-specific primers were designed to be complementary to cytosine on CpG sites whereas unmethylation specific primers were complementary to uracil on CpG sites. Primers were designed with MethPrimer software using input sequence −1000 to +900 bp of the mouse *klotho* start codon. A PCR product of genomic DNA that was not bisulfite converted was generated using primers located in the promoter region of *klotho* and used as input control. The methylation index was calculated as $2^{-}$(Ct of input − Ct of methylated or unmethylated primers). Primer sequences are listed in Table 1.

### Targeted bisulfite sequencing

Because hypermethylation at the *klotho* TSS is important in its silencing, we sequenced Ch5: 150952090–150953510 (−627 to +793 of the *klotho* start codon) (14,22). All 116 CpG sites within this region were covered by targeted bisulfite sequencing. Hamstrings from 3-month-old C57 and *mdx* mice were digested with 0.5 mg/ml proteinase K overnight at 55°C. Genomic DNA was purified using phenol–chloroform–isoamyl alcohol (25:24:1) before bisulfite treatment and sequencing. Methylation status of CpG sites in the specified regions of interest (ROI) was assayed using sodium bisulfite-converted DNA-specific primers (designed by Zymo Research, Irvine, CA) using proprietary software. All primers were then tested using real-time PCR with 1 ng of bisulfite-converted control DNA, in duplicate individual reactions.

Following primer validation, samples were bisulfite converted using the EZ DNA Methylation-Lightning Kit (Zymo) according to the manufacturer's instructions. Multiplex amplification of all samples using ROI-specific primer pairs and the Fluidigm Access ArrayTM System was performed according to the manufacturer's instructions. The resulting amplicons were pooled, purified (ZR-96 DNA Clean & Concentrator—ZR) and then prepared for sequencing using a MiSeq V2 300 bp reagent kit and paired-end sequencing protocol according to the manufacturer's guidelines.

### Targeted sequence alignments and data analysis

Sequence reads were identified using Illumina base-calling software and aligned to the reference genome using Bismark (http://www.bioinformatics.babraham.ac.uk/projects/bismark/), last accessed April 20, 2016, an aligner optimized for bisulfite sequence data and methylation calling (55). The methylation level of each sampled cytosine was estimated as the number of reads reporting a C, divided by the total number of reads reporting a C or T. The presence of DMR in the *klotho* promoter region was assessed using the R package Biseq (56,57).

### Cluster analysis of CpG methylation

The possibility that wild-type and *mdx* samples could be grouped separately according to their CpG methylation status in the *klotho* promoter region was assessed by hierarchical cluster analysis using the R package methylKit and single-linkage method (57).

### Chromatin immunoprecipitation

$C_2C_{12}$ cells were trypsinized to detach them from the culture dishes and then fixed in 1.1% formaldehyde for 15 min. The fixed chromatin was sheared using a Q800R1 sonication system at 20% amp, 15 s on, 15 s off for 24 cycles to reach fragment size of ∼500 bp. Whole muscle tissue that was used for ChIP was homogenized with a mortar and pestle cooled with liquid nitrogen. Samples were transferred to a pre-chilled centrifuge tube and fixed with 1.1% formaldehyde for 15 min. Fixed chromatin from muscle tissue was sheared by sonication at 40% amp, 15 s on, 30 s off for 26 cycles to reach fragment size of ∼500 bp. Ten micrograms of fixed chromatin from each sample was incubated with 2 μg anti-H3K9ac, anti-H3K9me2, anti-H3K79me2 or mouse IgG (Abcam) as negative control overnight. Protein A beads (Abcam) were washed and added to each sample. Each beads-chromatin mix was then washed three times with wash buffer, decrosslinked with 40 μg of proteinase K for 2 h at 55°C and then purified with phenol–chloroform–isoamyl alcohol (25:24:1). DNA was precipitated in 2.6× volume of 100% ethanol and diluted with 23 μl Tris–EDTA buffer. For an input control, 5 μg of fixed chromatin was directly decrosslinked and purified with phenol–chloroform–isoamyl alcohol. DNA concentration of the solution was measured; 50 ng of DNA was used in each PCR reaction.

### qPCR of ChIP samples

11.5 μl of each ChIP product or 50 ng of input DNA was used for *klotho* PCR. The primers were designed to specifically target *klotho* promoter region ch5:150952159–150952358 (−558 to −359 of *klotho* start codon) (Table 1). The results were calculated by percent input method.

### Menadione treatment of muscle cells

$C_2C_{12}$ myoblasts were seeded on 100 mm cell culture dishes at $2.5 \times 10^5$ cells per dish. Myoblasts were maintained in DMEM containing 10% FBS, penicillin and streptomycin at 37 °C in 5% $CO_2$. Culture medium was changed daily until cells reached 90% confluence. The cells were differentiated overnight in FBS-free DMEM containing 0, 7.5 or 15 μM menadione. On the next day (Day 1), the culture medium was changed into 10% FBS DMEM with appropriate menadione concentration. For the following 3 days, 10% FBS was changed every 24 h with appropriate menadione concentration. On Day 4, cells were collected for RNA, DNA methylation and histone modification analysis.

### Primary myoblast culture preparation

Primary myoblast cultures were prepared from 8-week-old *mdx* or wild-type mice as described previously (58). Hindlimb and forelimb muscles were removed and rinsed in Dulbecco's phosphate buffered saline (DPBS). Muscles were minced to a coarse slurry and digested in 2 ml enzyme buffer (2.4 U/ml dispase, type II (Invitrogen), 1% collagenase, type II (Invitrogen), 2.5 mM

$CaCl_2$) per mg muscle for 45 min at 37°C with gentle trituration each 15 min using a 25 or 5 ml serological pipet. The digestate was passed through 70 μm mesh filters and cells were pelleted at 350*g* for 5 min. Cells were resuspended in growth medium (Hams F10 (Sigma), 20% FBS (Omega), 2.5 ng/ml bFGF (Sigma), 200 U/ml penicillin and 200 μg/ml streptomycin (Life Technologies)) and pre-plated for 20–30 min to remove fibroblasts. Enriched myoblasts were plated on culture dishes coated with 0.01% collagen, type I (Life Technologies) and 2% gelatin and maintained at 37°C in 5% $CO_2$ with medium changes on alternate days. Myoblasts were passed once before stimulation.

## Assays for KL effects on myoblast proliferation

Primary myoblasts were seeded at $4 \times 10^4$ (*mdx*), or $2 \times 10^4$ (wild-type) cells per well in 12-well plates that were coated with collagen type I and gelatin and maintained in growth medium at 37°C in 5% $CO_2$ for 24 h before stimulation. The cultures were stimulated with either heparin only (10 μg/ml), KL (1 μg/ml) + heparin, FGF-23 (0.5 μg/ml) + heparin, or KL, FGF-23 and heparin in growth medium at 24 and 48 h post-plating. Following 48 h of stimulation, myoblast cultures were 80–90% confluent and released with 0.5 ml of 0.05% trypsin–EDTA (Life Technologies), washed with DPBS and stained with trypan blue (Life Technologies) for counting.

$C_2C_{12}$ myoblasts were also seeded in wells of six-well plates at $6 \times 10^4$ cells per well and maintained in DMEM containing 10% FBS, penicillin and streptomycin at 37 °C in an atmosphere of 5% $CO_2$. The cells were attached and ∼30% confluent 24 h after plating. Cells were stimulated as described for primary cultures. Five replicate wells were stimulated per treatment condition. Myoblasts were ∼90% confluent and not fused when they were collected 24 h following the second stimulation. Cells were released with 1 ml 0.05% trypsin–EDTA, washed with PBS and stained with trypan blue for counting.

We also assayed whether the delivery sequence of the individual, stimulation factors affected myoblast proliferation by introducing the factors in alternating succession. Myoblasts were seeded in six-well plates, stimulated, collected and counted following the schedule and dosing described above. One group of myoblast cultures was stimulated with KL/Hep at 24 h, followed by FGF/Hep at 48 h. A second group of myoblast cultures was stimulated with FGF/Hep at 24 h, followed by KL/Hep at 48 h. Control groups of Hep and KL/FGF/Hep were included to verify previous effects of stimulation on proliferation.

Proliferation of stimulated myoblasts was also measured by Ki67 staining. Myoblasts were seeded on sterile, glass coverslips coated with 2% gelatin in 60 mm dishes at 120 000 cells per dish. The cells were ∼30% confluent 24 h after plating. Myoblasts were stimulated with Hep, KL/Hep, FGF/Hep and KL/FGF/Hep following the schedule and dosing described previously. At 24 h following the second stimulation, coverslips with myoblasts were washed three times with PBS, fixed in cold, 100% methanol for 15 min and washed again with PBS. Coverslips were then incubated in 0.3% $H_2O_2$ in PBS for 10 min to quench endogenous peroxidases, washed in PBS and blocked in 3% BSA buffer (described above) for 30 min. Following a PBS wash, coverslips were incubated with goat anti-Ki67 (1:25; clone M-19, Santa Cruz Biotechnology) for 2 h at room temperature. Coverslips were washed three times with PBS before and after a 30 min incubation with biotin-conjugated anti-goat IgG (1:200; Vector Laboratories) and a subsequent, 30 min incubation with avidin–HRP (1:1000; Vector Laboratories). Red staining for Ki67 was visualized using the peroxidase substrate 3-amino-9-ethylcarbazole.

## Assays for KL effects on muscle cell death and apoptosis

Stimulated myoblasts were stained with annexin V or propidium iodide to determine whether cell viability was affected by the stimulation protocol. $C_2C_{12}$ myoblasts were seeded in 60 mm dishes at 120 000 cells per dish. Myoblasts were stimulated with Hep, KL/Hep, FGF/Hep and KL/FGF/Hep following the schedule and dosing described previously with triplicate plates per condition for each stain. To ensure that any detached, potentially apoptotic cells were detected, the culture medium was collected. The remaining, attached myoblasts were released with 2 ml of trypsin–EDTA as described previously and added to the collected medium. Myoblasts were pelleted and washed in PBS to prepare cells for staining in suspension. Pellets were resuspended in annexin-V-FITC (1:100 in 1X binding buffer; Trevigen, Gaithersburg, MD) and incubated 15 min at room temperature while protected from light. Stained myoblasts were washed with binding buffer, applied to glass slides drop-wise and mounted for analysis. The remaining myoblast pellets were stained with propidium iodide (1:10 in 1X binding buffer; Trevigen) following an identical protocol.

## Assay for KL effects on muscle growth

Myoblasts were seeded in six-well plates at 120 000 cells per well, grown to confluence with culture medium changes on alternate days and differentiated as described above. Myotubes were stimulated with Hep, KL/Hep, FGF/Hep and KL/FGF/Hep at 24 and 48 h after differentiation following the previously described dosing with five replicates per treatment. Cells were collected in reducing sample buffer (80 mM Tris–HCl pH 6.8, 0.1 M dithiothreitol, 70 mM sodium dodecyl sulfate, 1.0 mM glycerol) with protease inhibitor cocktail (1:100, Sigma) 24 h after the second stimulation. Protein concentration per well was determined as described previously (59).

## Muscle function testing

We assayed the effects of *klotho* transgene expression on mouse function by measuring running time on a treadmill (Exer 3/6 treadmill; Columbus Instruments) until exhaustion. Eight-month-old mice were first acclimated to the treadmill by allowing them to run voluntarily at low speed (4 m/s). They were subsequently tested at a treadmill speed set at 8 m/s on a +10° incline until exhausted. Exhaustion was identified at the point when mice would rest on a grid delivering electrical shocks at the bottom of the treadmill (3.4 mA for 200 ms at 3 Hz), rather than continue running. We also used a modified wire-hang test to assess mouse strength (54). Mice were tested for hang-time while holding onto a horizontal wire, with a 1 min rest intervals between trials. The longest time of the three trials was used for comparison to other mice.

## Fiber size and number

Frozen, cross-sections of tibialis anterior muscles were sectioned at the midbelly of muscles and used for fiber cross-sectional area measurements, fiber number counts and measurements of variance of cross-sectional areas within treatment groups. Sections were stained with a hematoxylin solution, all

fibers were counted, and the cross-sectional area of 500 fibers was measured using a digital imaging system (Bioquant).

### Assay for fiber damage

Injured muscle fibers were identified by the presence of mouse IgG in the cytoplasm, indicating that the fibers had membrane lesions large enough to allow large extracellular proteins to diffuse into the cell. Frozen cross-sections of quadriceps muscle were incubated for 30 min in 3% BSA and 0.05% Tween-20 diluted in 50 mM Tris–HCl pH 7.6 containing 150 mM NaCl. The sections were then washed in PBS and then incubated in biotinylated anti-mouse IgG (1:200; Vector) for 1 h, washed in PBS and then incubated for 30 min with avidin-conjugated HRP (1:1000; Vector). Immunolabeled fibers were then visualized using a peroxidase substrate kit (Vector). Injured fibers were then identified microscopically and their numbers expressed relative to the total number of fibers present in the muscle cross-section.

### Assay for central nucleation

The proportion of fibers containing central nuclei, an indicator of previous injury and regeneration, was determined in frozen, hematoxylin-stained cross-sections of entire quadriceps muscles. Central-nucleation was expressed as the ratio of central nucleated fibers relative to the entire population of fibers sampled for each muscle.

### Assay of muscle connective tissue content

The volume fraction of muscle that was occupied by collagen type 1 or collagen type 3 was determined by overlaying a $10 \times 10$ eye-piece μm grid on microscopic images of cross-sections of entire muscles that were immunolabeled with antibodies to collagens type 1 or type 3. The percentage of grid intercepts that overlaid antibody-labeled connective tissue relative to total grid intercepts was determined to assess connective tissue volume fraction.

## Statistics

Data are presented as mean ± S.E.M. One-way analysis of variance was used to test whether differences between groups were significant at $P < 0.05$. Significant differences between groups were identified using Tukey's *post hoc* test.

## Supplementary Material

Supplementary Material is available at HMG online.

## Acknowledgements

The authors thank David Rangel and Katherine Wen for expert assistance in preparing tissue for histology and immunohistochemistry and thank Kevin Lloyd and Ellen Snavely for their performance of QPCR analyses.

## Funding

National Institutes of Health (AR062579, AR066036, AG041147 and AR066817) to J.G.T. and (AR065845) to S.S.W.

*Conflict of Interest statement* None declared.

## References

1. Hoffman, E.P., Brown, R.H., Jr and Kunkel, L.M. (1987) Dystrophin: the protein product of the Duchenne muscular dystrophy locus. *Cell*, **5**, 919–928.
2. Ervasti, J.M., Ohlendieck, K., Kahl, S.D., Gaver, M.G. and Campbell, K.P. (1990) Deficiency of a glycoprotein component of the dystrophin complex in dystrophic muscle. *Nature*, **345**, 315–319.
3. Brenman, J.E., Chao, D.S., Xia, H., Aldape, K. and Bredt, D.S. (1995) Nitric oxide synthase complexed with dystrophin and absent from skeletal muscle sarcolemma in Duchenne muscular dystrophy. *Cell*, **82**, 743–752.
4. Chang, W.J., Iannaccone, S.T., Lau, K.S., Masters, B.S., McCabe, T.J., McMillan, K., Padre, R.C., Spencer, M., Tidball, J.G. and Stull, J.T. (1996) Neuronal nitric oxide synthase and dystrophin-deficient muscular dystrophy. *Proc. Natl Acad. Sci. USA*, **93**, 9142–9147.
5. Tidball, J.G. and Wehling-Henricks, M. (2014) Nitric oxide synthase deficiency and the pathophysiology of muscular dystrophy. *J. Physiol.*, **592**, 4627–4638.
6. Wehling, M., Spencer, M.J. and Tidball, J.G. (2001) A nitric oxide synthase transgene ameliorates muscular dystrophy in *mdx* mice. *J. Cell Biol.*, **155**, 123–131.
7. Colussi, C., Gurtner, A., Rosati, J., Illi, B., Ragone, G., Piaggio, G., Moggio, M., Lamperti, C., D'Angelo, G., Clementi, E. *et al.* (2009) Nitric oxide deficiency determines global chromatin changes in Duchenne muscular dystrophy. *FASEB J.*, **23**, 2131–2141.
8. Minetti, G.C., Colussi, C., Adami, R., Serra, C., Mozzetta, C., Parente, V., Fortuni, S., Straino, S., Sampaolesi, M., Di Padova, M. *et al.* (2006) Functional and morphological recovery of dystrophic muscles in mice treated with deacetylase inhibitors. *Nat. Med.*, **12**, 1147–1150.
9. Consalvi, S., Saccone, V., Giordani, L., Minetti, G., Mozzetta, C. and Puri, P.L. (2011) Histone deacetylase inhibitors in the treatment of muscular dystrophies: epigenetic drugs for genetic diseases. *Mol. Med.*, **17**, 457–465.
10. Kuro-o, M., Matsumura, Y., Aizawa, H., Kawaguchi, H., Suga, T., Utsugi, T., Ohyama, Y., Kurabayashi, M., Kaname, T., Kume, E. *et al.* (1997) Mutation of the mouse Klotho gene leads to a syndrome resembling ageing. *Nature*, **390**, 45–51.
11. Matsumura, Y., Aizawa, H., Shiraki-Iida, T., Nagai, R., Kuro-o, M. and Nabeshima, Y. (1998) Identification of the human Klotho gene and its two transcripts encoding membrane and secreted Klotho protein. *Biochem. Biophys. Res. Commun.*, **242**, 626–630.
12. Li, S.A., Watanabe, M., Yamada, H., Nagai, A., Kinuta, M. and Takei, K. (2004) Immunohistochemical localization of Klotho protein in brain, kidney, and reproductive organs of mice. *Cell Struct. Funct.*, **29**, 91–99.
13. Phelps, M., Pettan-Brewer, C., Ladiges, W. and Yablonka-Reuveni, Z. (2013) Decline in muscle strength and running endurance in Klotho deficient C57BL/6 mice. *Biogerontology*, **14**, 729–739.
14. Sun, C.Y., Chang, S.C. and Wu, M.S. (2012) Suppression of Klotho expression by protein-bound uremic toxins is associated with increased DNA methyltransferase expression and DNA hypermethylation. *Kidney Int.*, **81**, 640–650.
15. Chen, J., Zhang, X., Zhang, H., Lin, J., Zhang, C., Wu, Q. and Ding, X. (2013) Elevated Klotho promoter methylation is associated with severity of chronic kidney disease. *PLoS One*, **8**, e79856.

16. Lee, J., Jeong, D.J., Kim, J., Lee, S., Park, J.H., Chang, B., Jung, S.I., Yi, L., Han, Y., Yang, Y. *et al.* (2010) The anti-aging gene KLOTHO is a novel target for epigenetic silencing in human cervical carcinoma. *Mol. Cancer*, **9**, 109.
17. Pan, J., Zhong, J., Gan, L.H., Chen, S.J., Jin, H.C., Wang, X. and Wang, L.J. (2011) Klotho, an anti-senescence related gene, is frequently inactivated through promoter hypermethylation in colorectal cancer. *Tumour Biol.*, **32**, 729–735.
18. Rubinek, T., Shulman, M., Israeli, S., Bose, S., Avraham, A., Zundelevich, A., Evron, E., Gal-Yam, E.N., Kaufman, B. and Wolf, I. (2012) Epigenetic silencing of the tumor suppressor Klotho in human breast cancer. *Breast Cancer Res. Treat.*, **133**, 649–657.
19. Xin, Y.J., Yuan, B., Yu, B., Wang, Y.Q., Wu, J.J., Zhou, W.H. and Qiu, Z. (2015) Tet1-mediated DNA demethylation regulates neuronal cell death induced by oxidative stress. *Sci. Rep.*, **5**, 7645.
20. Irifuku, T., Doi, S., Sasaki, K., Doi, T., Nakashima, A., Ueno, T., Yamada, K., Arihiro, K., Kohno, N. and Masaki, T. (2016) Inhibition of H3K9 histone methyltransferase G9a attenuates renal fibrosis and retains Klotho expression. *Kidney Int.*, **89**, 147–157.
21. Chamberlain, J.S., Metzger, J., Reyes, M., Townsend, D. and Faulkner, J.A. (2007) Dystrophin-deficient mdx mice display a reduced life span and are susceptible to spontaneous rhabdomyosarcoma. *FASEB J.*, **2**, 2195–2204.
22. Azuma, M., Koyama, D., Kikuchi, J., Yoshizawa, H., Thasinas, D., Shiizaki, K., Kuro-o, M., Furukawa, Y. and Kusano, E. (2012) Promoter methylation confers kidney-specific expression of the Klotho gene. *FASEB J.*, **26**, 4264–4274.
23. Turek-Plewa, J. and Jagodzinski, P.P. (2005) The role of mammalian DNA methyltransferases in the regulation of gene expression. *Cell. Mol. Biol. Lett.*, **10**, 631–647.
24. Mitobe, M., Yoshida, T., Sugiura, H., Shirota, S., Tsuchiya, K. and Nihei, H. (2005) Oxidative stress decreases Klotho expression in a mouse kidney cell line. *Nephron Exp. Nephrol.*, **101**, e67–e74.
25. Franco, A.A., Odom, R.S. and Rando, T.A. (1999) Regulation of antioxidant enzyme gene expression in response to oxidative stress and during differentiation of mouse skeletal muscle. *Free Radic. Biol. Med.*, **27**, 1122–1132.
26. Samengo, G., Avik, A., Fedor, B., Whittaker, D., Myung, K.H., Wehling-Henricks, M. and Tidball, J.G. (2012) Age-related loss of nitric oxide synthase in skeletal muscle causes reductions in calpain S-nitrosylation that increase myofibril degradation and sarcopenia. *Aging Cell*, **11**, 1036–1045.
27. Wu, X., Ge, H., Gupte, J., Weiszmann, J., Shimamoto, G., Stevens, J., Hawkins, N., Lemon, B., Shen, W., Xu, J. *et al.* (2007) Co-receptor requirements for fibroblast growth factor-19 signaling. *J. Biol. Chem.*, **282**, 29069–29072.
28. Kurosu, H., Ogawa, Y., Miyoshi, M., Yamamoto, M., Nandi, A., Rosenblatt, K.P., Baum, M.G., Schiavi, S., Hu, M.C., Moe, O.W. and Kuro-o, M. (2006) Regulation of fibroblast growth factor-23 signaling by Klotho. *J. Biol. Chem.*, **281**, 6120–6123.
29. Brack, A.S., Conboy, M.J., Roy, S., Lee, M., Kuo, C.J., Keller, C. and Rando, T.A. (2007) Increased Wnt signaling during aging alters muscle stem cell fate and increases fibrosis. *Science*, **317**, 807–810.
30. Biressi, S., Miyabara, E.H., Gopinath, S.D., Carlig, P.M. and Rando, T.A. (2014) A Wnt-TGFbeta2 axis induces a fibrogenic program in muscle stem cells from dystrophic mice. *Sci. Transl. Med.*, **6**, 267ra176.
31. Vidal, B., Serrano, A.L., Tjwa, M., Suelves, M., Ardite, E., De Mori, R., Baeza-Raja, B., Martínez de Lagrán, M., Lafuste, P., Ruiz-Bonilla, V. *et al.* (2008) Fibrinogen drives dystrophic muscle fibrosis via a TGFbeta/alternative macrophage activation pathway. *Genes Dev.*, **22**, 1747–1752.
32. Lemos, D.R., Babaeijandaghi, F., Low, M., Chang, C.K., Lee, S.T., Fiore, D., Zhang, R.H., Natarajan, A., Nedospasov, S.A. and Rossi, F.M. (2015) Nilotinib reduces muscle fibrosis in chronic muscle injury by promoting TNF-mediated apoptosis of fibro/adipogenic progenitors. *Nat. Med.*, **21**, 786–794.
33. Wehling-Henricks, M., Jordan, M.C., Gotoh, T., Grody, W.W., Roos, K.P. and Tidball, J.G. Arginine metabolism by macrophages promotes cardiac and muscle fibrosis in *mdx* muscular dystrophy. *PLoS One*, **5**, e10763.
34. Wang, Y., Wehling-Henricks, M., Samengo, G. and Tidball, J.G. (2015) Increases of M2a macrophages and fibrosis in aging muscle are influenced by bone marrow aging and negatively regulated by muscle-derived nitric oxide. *Aging Cell*, **14**, 678–688.
35. Shiraki-Iida, T., Aizawa, H., Matsumura, Y., Sekine, S., Iida, A., Anazawa, H., Nagai, R., Kuro-o, M. and Nabeshima, Y. (1998) Structure of the mouse Klotho gene and its two transcripts encoding membrane and secreted protein. *FEBS Lett.*, **424**, 6–10.
36. Chen, C.D., Podvin, S., Gillespie, E., Leeman, S.E. and Abraham, C.R. (2007) Insulin stimulates the cleavage and release of the extracellular domain of Klotho by ADAM10 and ADAM17. *Proc. Natl Acad. Sci. USA*, **104**, 19796–19801.
37. Fry, C.S., Lee, J.D., Mula, J., Kirby, T.J., Jackson, J.R., Liu, F., Yang, L., Mendias, C.L., Dupont-Versteegden, E.E., McCarthy, J.J. and Peterson, C.A. (2015) Inducible depletion of satellite cells in adult, sedentary mice impairs muscle regenerative capacity without affecting sarcopenia. *Nat. Med.*, **21**, 76–80.
38. Heslop, L., Morgan, J.E. and Partridge, T.A. (2000) Evidence for a myogenic stem cell that is exhausted in dystrophic muscle. *J. Cell Sci.*, **113**, 2299–2308.
39. Sugiura, H., Yoshida, T., Shiohira, S., Kohei, J., Mitobe, M., Kurosu, H., Kuro-o, M., Nitta, K. and Tsuchiya, K. (2012) Reduced Klotho expression level in kidney aggravates renal interstitial fibrosis. *Am. J. Physiol. Renal Physiol.*, **302**, F1252–F1264.
40. Doi, S., Zou, Y., Togao, O., Pastor, J.V., John, G.B., Wang, L., Shiizaki, K., Gotschall, R., Schiavi, S., Yorioka, N. *et al.* (2011) Klotho inhibits transforming growth factor-beta1 (TGF-beta1) signaling and suppresses renal fibrosis and cancer metastasis in mice. *J. Biol. Chem.*, **286**, 8655–8665.
41. Satoh, M., Nagasu, H., Morita, Y., Yamaguchi, T.P., Kanwar, Y.S. and Kashihara, N. (2012) Klotho protects against mouse renal fibrosis by inhibiting Wnt signaling. *Am. J. Physiol. Renal Physiol.*, **303**, F1641–F1651.
42. Saito, Y., Nakamura, T., Ohyama, Y., Suzuki, T., Iida, A., Shiraki-Iida, T., Kuro-o, M., Nabeshima, Y., Kurabayashi, M. and Nagai, R. (2000) In vivo Klotho gene delivery protects against endothelial dysfunction in multiple risk factor syndrome. *Biochem. Biophys. Res. Commun.*, **276**, 767–772.
43. Yamazaki, M., Minota, S., Sakurai, H., Miyazono, K., Yamada, A., Kanazawa, I. and Kawai, M. (1994) Expression of transforming growth factor-beta 1 and its relation to endomysial fibrosis in progressive muscular dystrophy. *Am. J. Pathol.*, **144**, 221–226.
44. Chen, T.H., Kuro-o, M., Chen, C.H., Sue, Y.M., Chen, Y.C., Wu, H.H. and Cheng, C.Y. (2013) The secreted Klotho protein restores phosphate retention and suppresses accelerated aging in Klotho mutant mice. *Eur. J. Pharmacol.*, **698**, 67–73.
45. Liu, H., Fergusson, M.M., Castilho, R.M., Liu, J., Cao, L., Chen, J., Malide, D., Rovira, I.I., Schimel, D., Kuo, C.J. *et al.* (2007)

Augmented Wnt signaling in a mammalian model of accelerated aging. *Science*, **317**, 803–806.
46. Roberts, A.B., Sporn, M.B., Assoian, R.K., Smith, J.M., Roche, N.S., Wakefield, L.M., Heine, U.I., Liotta, L.A., Falanga, V., Kehrl, J.H. and Fauci, A.S. (1986) Transforming growth factor type beta: rapid induction of fibrosis and angiogenesis in vivo and stimulation of collagen formation in vitro. *Proc. Natl Acad. Sci. USA*, **83**, 4167–4171.
47. Raghow, R., Postlethwaite, A.E., Keski-Oja, J., Moses, H.L. and Kang, A.H. (1987) Transforming growth factor-beta increases steady state levels of type I procollagen and fibronectin messenger RNAs posttranscriptionally in cultured human dermal fibroblasts. *J. Clin. Invest.*, **79**, 1285–1288.
48. Uezumi, A., Fukada, S., Yamamoto, N., Takeda, S. and Tsuchida, K. (2010) Mesenchymal progenitors distinct from satellite cells contribute to ectopic fat cell formation in skeletal muscle. *Nat. Cell Biol.*, **12**, 143–152.
49. Joe, A.W., Yi, L., Natarajan, A., Le Grand, F., So, L., Wang, J., Rudnicki, M.A. and Rossi, F.M. (2010) Muscle injury activates resident fibro/adipogenic progenitors that facilitate myogenesis. *Nat. Cell Biol.*, **12**, 153–163.
50. Spencer, M., Walsh, C.M., Dorshkind, K.A., Rodriguez, E.M. and Tidball, J.G. (1997) Myonuclear apoptosis in dystrophic mdx muscle occurs by perforin-mediated cytotoxicity. *J. Clin. Invest.*, **99**, 2745–2751.
51. Amalfitano, A. and Chamberlain, J.S. (1996) The mdx-amplification-resistant mutation system assay, a simple and rapid polymerase chain reaction-based detection of the mdx allele. *Muscle Nerve*, **19**, 1549–1553.
52. Nolan, T., Hands, R.E. and Bustin, S.A. (2006) Quantification of mRNA using real-time RT-PCR. *Nat. Protoc.*, **1**, 1559–1582.
53. Bustin, S.A., Benes, V., Garson, J.A., Hellemans, J., Huggett, J., Kubista, M., Mueller, R., Nolan, T., Pfaffl, M.W., Shipley, G.L. *et al.* (2009) The MIQE guidelines: minimum information for publication of quantitative real-time PCR experiments. *Clin. Chem.*, **55**, 611–622.
54. Villalta, S.A., Rinaldi, C., Deng, B., Liu, G., Fedor, B. and Tidball, J.G. (2011) Interleukin-10 reduces the pathology of *mdx* muscular dystrophy by deactivating M1 macrophages and modulating macrophage phenotype. *Hum. Mol. Genet.*, **20**, 790–805.
55. Krueger, F. and Andrews, S.R. (2011) Bismark: a flexible aligner and methylation caller for Bisulfite-Seq applications. *Bioinformatics*, **27**, 1571–1572.
56. Hebestreit, K., Dugas, M. and Klein, H.U. (2013) Detection of significantly differentially methylated regions in targeted bisulfite sequencing data. *Bioinformatics*, **29**, 1647–1653.
57. Akalin, A., Kormaksson, M., Li, S., Garrett-Bakelman, F.E., Figueroa, M.E., Melnick, A. and Mason, C.E. (2012) methylKit: a comprehensive R package for the analysis of genome-wide DNA methylation profiles. *Genome Biol.*, **13**, R87.
58. Rando, T.A. and Blau, H.M. (1994) Primary mouse myoblast purification, characterization and transplantation for cell-mediated gene therapy. *J. Cell Biol.*, **125**, 1275–1287.
59. Minamide, L.S. and Bamburg, J.R. (1990) A filter paper dye-binding assay for quantitative determination of protein without interference from reducing agents or detergents. *Anal. Biochem.*, **190**, 66–70.